

## Response to anonymous referee #2 (R2)

### i) Grain-size data:

I still think that Figure 2 is not appropriate for visualizing the grain-size results. Even if it will be in landscape format in the final paper version, the grain-size results are simply too small in this figure illustrating the entire sediment sequence. I therefore persist on my previous proposition to add a zoom over a 10-20 cm long core interval (or whatever length seems to be best, hard to see) to demonstrate the grain sizes within flood layers and within the background sediment. There are former Wilhelm et al. papers that do this nicely, thus it will not be much work. It looks like adding the zoom to Figure 2 is difficult. The better solution is probably to add another figure. For the whole discussion about the best proxy for flood intensity this is definitely worth it.

>> According to the reviewer comment, a new figure (Fig. S1) was added to the Supplementary Material to show a zoom of the grain-size data.

ii) L. 162: What do you mean with 'grain-size proxies'? This is too vague. Either simply say grain-size analysis or elaborate more what you imply with 'proxies' in this context.

>> 'Proxies' was changed to 'analysis' as suggested.

iii) L. 177: 'appears' instead of 'appeared'

>> This has been changed.

### 3) XRF counts as quantitative indication of element concentrations

There is still one sentence that caught my attention:

L. 158: 'The areas of the element peaks obtained are proportional to the concentrations of each element (Tachikawa et al., 2011).'

This is a highly concluding sentence, implying that this situation applies to all sediment sequences and excluding all possible matrix, pore water, density etc. effects on the XRF counts. In addition, this sentence is supported by only one single study.

You should therefore reformulate and possibly elaborate a bit more.

The present sentence could for instance be replaced with: 'Several studies could demonstrate that counts received from XRF core scanning are proportional to element concentrations if no important matrix effects due to pronounced lithology changes or variations of pore water volume and chemical composition are present (refs).'

-> Cartapanis et al. 2011, Paleoceanography, would be another study using an ITRAX scanner and applying calibration of counts through ICP-MS measurements.

However, I would propose you also search for a good reference working with lacustrine and not with marine sediments.

>> The sentence was changed to the one the reviewer suggested and two references specific to lake sediments added as suggested by the reviewer.

### Figure 4:

I am still wondering what MP stands for. Maximal peak? Would be a bit strange as a peak is usually maximal. Why don't you just omit the abbreviations and write the terms out ('Chernobyl' and 'Bomb Peak'). There is enough space in the figure.

>> This has been changed as suggested

# 1 Frequency and intensity of palaeofloods at the interface of 2 Atlantic and Mediterranean climate domains

3  
4 **B. Wilhelm<sup>1,2</sup>, H. Vogel<sup>2</sup>, C. Crouzet<sup>3,4</sup>, D. Etienne<sup>5</sup>, F.S. Anselmetti<sup>2</sup>**

5  
6 [1]{Univ. Grenoble Alpes, LTHE, F-38000 Grenoble, France }

7 [2]{Institute of Geological Sciences and Oeschger Centre for Climate Change Research,  
8 Univ. of Bern, CH-3012 Bern, Switzerland }

9 [3]{Univ. Savoie Mont Blanc, ISTerre, F-73376 Le Bourget-du-Lac, France }

10 [4]{CNRS, ISTerre, F-73376 Le Bourget-du-Lac, France }

11 [5]{UMR INRA 42 CARRTEL, Univ. Savoie Mont Blanc, F-73376 Le Bourget du Lac,  
12 France }

13 Correspondence to: B. Wilhelm (bruno.wilhelm@ujf-grenoble.fr)

## 14 15 **Abstract**

16 The long-term response of the flood activity to both Atlantic and Mediterranean climatic  
17 influences was explored by studying a lake sequence (Lake Foréant) of the Western European  
18 Alps. High-resolution sedimentological and geochemical analysis revealed 171 event layers,  
19 168 of which result from past flood events over the last millennium. The layer thickness was  
20 used as a proxy of intensity of past floods. Because the Foréant palaeoflood record is in  
21 agreement with the documented variability of historical floods resulting from local and  
22 mesoscale, summer-to-autumn convective events, it is assumed to highlight changes in flood  
23 frequency and intensity related to such events typical of both Atlantic (local events) and  
24 Mediterranean (meso-scale events) climatic influences. Comparing the Foréant record with  
25 other Atlantic-influenced and Mediterranean-influenced regional flood records highlights a  
26 common feature in all flood patterns that is a higher flood frequency during the cold period of  
27 the Little Ice Age (LIA, AD 1300-1900). In contrast, high-intensity flood events are apparent  
28 during both, the cold LIA and the warm Medieval Climate Anomaly (MCA, AD 950-1250).  
29 However, there is a tendency towards higher frequencies of high-intensity flood events during  
30 the warm MCA. The MCA extremes could mean that under the global warming scenario, we  
31 might see an increase in intensity (not in frequency). However, the flood frequency and  
32 intensity in course of 20<sup>th</sup> century warming trend did not change significantly. Uncertainties in

33 future evolution of flood intensity lie in the interpretation of the lack of 20<sup>th</sup> century extremes  
34 (transition or stable?) and the different climate forcing factors between the two periods  
35 (greenhouse gases vs. solar/volcanic eruptions).

36

37 **Key-words:** palaeoflood record, flood frequency, flood intensity, Atlantic influence,  
38 Mediterranean influence, last millennium

39

## 40 **1. Introduction**

41 Heavy rainfall events trigger mountain-river floods, one of the most significant natural  
42 hazards, causing widespread loss of life, damage to infrastructure and economic deprivation  
43 (e.g. Kundzewicz et al., 2014). This is especially the case for the Alpine area in Europe,  
44 where tourism and recent demographic development with an increasing population raise the  
45 vulnerability of infrastructure to natural hazards (e.g. Beniston and Stephenson 2004).  
46 Moreover, the current global warming is expected to lead to an intensification of the  
47 hydrological cycle and a modification of flood hazard (IPCC et al., 2013). Hence, a robust  
48 assessment of the future evolution of the flood hazard over the Alps becomes a crucial issue.

49 A main limitation for robust flood-hazard projections is the scarce knowledge on the  
50 underlying natural climate dynamics that lead to these extreme events (IPCC, 2013). Indeed,  
51 the stochastic nature and the rare occurrence of extreme events make the identification of  
52 trends based on instrumental data alone difficult (e.g. Lionello et al., 2012). One way of  
53 overcoming this issue is to extend flood series beyond observational data and compare these  
54 datasets with independent climatic and environmental forcing. In this purpose, many types of  
55 sedimentary archives have been studied (e.g. Luterbacher et al., 2012 and references therein).  
56 Among them lake sediments are being increasingly studied because they allow to reconstruct  
57 flood records long enough to identify the natural variability at different time scales (e.g.  
58 Noren et al., 2002; Osleger et al., 2009; Wilhelm et al., 2012a; Czymzik et al., 2013; Glur et  
59 al., 2013; Corella et al., 2014).

60 In the western Alps, many lake-sediment sequences have been studied to better assess the  
61 response of the flood activity to climate variability. These studies revealed higher flood  
62 frequency of mountain streams in many regions during multi-centennial cold phases such as  
63 the Little Ice Age (Giguet-Covex et al., 2012; Wilhelm et al., 2012a; 2013; Glur et al., 2013;  
64 Wirth et al., 2013b; Amann et al., 2015). However, regarding flood intensity/magnitude,

65 opposite patterns appear with the occurrence of the most extreme events during warmer  
66 periods in the north (Giguet-Covex et al., 2012; Wilhelm et al., 2012b; 2013), while they  
67 occurred during colder periods in the south (Wilhelm et al., 2012a; 2015). These north-south  
68 opposite flood patterns were explained by flood-triggering meteorological processes specific  
69 to distinct climatic influences: Atlantic in the north versus Mediterranean in the south. In the  
70 north-western part of the Alps, floods at high altitude are mainly triggered by local convective  
71 events (i.e. thunderstorms) and seem to mainly depend on the temperature that would  
72 strengthen vertical processes (e.g. Wilhelm et al., 2012b; 2013). In contrast, floods in the  
73 south are mostly triggered by mesoscale events and may strongly depend on pathways and  
74 intensity of storm-tracks (e.g. Trigo and Davis, 2000; Boroneant et al., 2006; Boudevillain et  
75 al., 2009). By analogy with these results over past warm periods, the mountain-flood hazard  
76 might be expected to increase in the north-western Alps, mainly because of an enhanced flood  
77 magnitude associated to stronger convective processes. Hence, better assessing the spatial  
78 extent of the Atlantic-influenced flood pattern at high-altitude appears a crucial issue to  
79 appropriately establish hazard mitigation plans and prevent high socio-economic damages.

80 In this context, the present study was designed to reconstruct the flood pattern at an  
81 intermediate situation between the north-western and south-western Alps, i.e. at the climate  
82 boundary between Atlantic and Mediterranean influences. This is undertaken by  
83 reconstructing a millennium-long flood chronicle from the sediment sequence of the high-  
84 altitude Lake Foréant located in the Queyras Massif (France).

85

## 86 **2. Regional setting**

87

### 88 **2.1. Hydro-climatic setting and historical flood record**

89 The Queyras massif is located in between the northern and southern French Alps where the  
90 climate is influenced by the Atlantic Ocean and the Mediterranean Sea (Fig. 1). As a result,  
91 the Queyras mountain range corresponds to a transition zone of Alpine precipitation patterns  
92 in the meteorological reanalyses (Durant et al., 2009; Plaut et al., 2009) and in the simulations  
93 (Frei et al., 2006; Rajczak et al., 2013). In the Queyras, heavy precipitation events are related  
94 to either local convective phenomena (i.e. summer thunderstorms) or mesoscale convective  
95 systems. The mesoscale systems called “Lombarde-Type” or “East Return” events occur  
96 mainly from late spring to fall and result from Mediterranean humid air masses flowing

97 northward into the Po Plain and then westward to the Queyras Massif (e.g. Gottardi et al.,  
98 2010; Parajka et al., 2010). The humid air masses are then vigorously uplifted with the steep  
99 topography of the Queyras massif, causing an abrupt cooling of the air masses and intense  
100 precipitations. Such mesoscale precipitation events, typical of the Mediterranean climate (e.g.  
101 Buzzi and Foschini, 2000; Lionello et al., 2012), affect extensive areas and may lead to  
102 catastrophic floods at a regional scale as shown in June 1957 or October 2000 over the  
103 Queyras massif (Arnaud-Fassetta and Fort, 2004). Other numerous past flood events were  
104 documented from studies of local historical records. These data have been compiled in a  
105 database managed by the ONF-RTM (<http://rtm-onf.ifn.fr/>). They show that the village of  
106 Ristolas (located 8 km downstream from Lake Foréant, Fig. 1C) has been affected at least 34  
107 times over the last 250 years by floods of the Guil River and its five main tributaries (see  
108 Supplementary Material).

109

## 110 **2.2. Lake Foréant and its tributaries**

111 Lake Foréant (2620 m a.s.l., 44°42'20"N, 6°59'00"E) is located in a cirque of 3 km<sup>2</sup> in the  
112 upper part of the Queyras Massif, adjacent to the Italian border (Fig. 1). It is located  
113 approximately 60 km north from Lake Allos and 100 km south-west from Lakes Blanc,  
114 whose hydro-climatic settings are characterized by the south-western and north-western flood  
115 pattern, respectively (Wilhelm et al., 2012a,b; Fig. 1B). The catchment rises up to 3210 m.  
116 a.s.l. and is made up of three lithologies from the Queyras schistes-lustrés nappe (e.g.  
117 Schwartz et al., 2009); (i) marble in the eastern part, (ii) calc-schist in the western part and  
118 (iii) a narrow band of arkose in between (Fig. 1D). The main stream of the catchment, the  
119 Torrent de Bouchouse, drains mainly the central band of arkose. Before entering the lake, this  
120 stream has built an alluvial plain (Fig. 1E). This suggests that the Bouchouse stream is a  
121 major source of sediment entering the lake. In addition, two minor and non-permanent  
122 streams drain the western part of the catchment. In contrast, they enter the lake through only  
123 small deltas compared to the Bouchouse inflow area, suggesting limited detrital inputs. There  
124 is no evidence that the catchment was glaciated in the past, i.e. no moraine or other glacial  
125 deposits occur. Thereby, detrital inputs only result from the erosion and transport of these  
126 lithologies. Detrital inputs from these streams are limited to summer and fall because the  
127 catchment is covered by snow and the lake is frozen from mid-November to the beginning of  
128 June. The Bouchouse stream flows downstream into the Guil River and reaches  
129 approximately 8 km further the village of Ristolas (Fig. 1C).

130

### 131 **3. Method**

132

#### 133 **3.1. Lake coring**

134 In summer 2013, a bathymetric survey was carried out on Lake Foréant and revealed a well-  
135 developed flat basin in the centre of the lake with a maximum water depth of 23.5 m (Fig.  
136 1E). An UWITEC gravity corer was used to retrieve four cores along a north-south transect in  
137 the axis of the two main inlets of the Bouchouse stream. Cores FOR13P3 and FOR13P4  
138 correspond to the proximal locations of the two different branches of the Bouchouse stream  
139 and aim at investigating their respective sediment inputs during floods. Cores FOR13P2 and  
140 FOR13P1 correspond to the depocenter and to the most distal position, i.e. the opposite slope  
141 to the Bouchouse inflows, respectively.

142

#### 143 **3.2. Core description and logging**

144 Cores were split lengthwise and the visual macroscopic features of each core were examined  
145 to identify the different sedimentary lithofacies. The stratigraphic correlation between the  
146 cores was then carried out based on these defined lithofacies. The stratigraphic correlation  
147 allows identifying the depositional pattern of the event layers within the lake basin.  
148 Depositional patterns of event layers may help to decipher their trigger, i.e. mass-movements  
149 vs. flood events (e.g. Sturm and Matter, 1978; Wilhelm et al., 2012b; Van Daele et al., 2015).

150 High-resolution color line scans and gamma-ray attenuation bulk density measurements were  
151 carried out on a Geotek<sup>TM</sup> multisensor core-logger (Institute of Geological Sciences,  
152 University of Bern). Bulk density was used as a proxy of event layers, e.g. flood layers,  
153 characterized by higher density due to the high amount of detrital material (e.g. Støren et al.,  
154 2010; Gilli et al., 2012; Wilhelm et al., 2012b).

155 Geochemical analysis and X-ray imaging were carried out using an Itrax<sup>TM</sup> (Cox Analytical  
156 Systems) X-ray fluorescence (XRF) core scanner (Institute of Geological Sciences, University  
157 of Bern), equipped with a Molybdenum tube (50 keV, 30 mA) with a 10-s count-time using  
158 sampling steps of 1 mm (XRF) and 0.2 mm (X-ray imaging). Several studies could  
159 demonstrate that counts received from XRF core scanning are proportional to element  
160 concentrations if no important matrix effects due to pronounced lithology changes or

161 variations of pore water volume and chemical composition are present (e.g. Kylander et al.,  
162 2013; Russell et al., 2014). Geochemical data were applied to identify event layers at high  
163 resolution through their higher content in detrital material (e.g. Arnaud et al., 2012; Wilhelm  
164 et al., 2012b; Czymzik et al., 2013; Swierczynski et al., 2013) and/or as high-resolution grain-  
165 size analysis (e.g. Cuven et al., 2010; Wilhelm et al., 2012a; 2013). Geochemical analyses  
166 were carried out on core FOR13P2. X-ray images highlighting the variability of the sediment  
167 density have been acquired for the four cores.

168 Grain size analyses on core FOR13P2 were performed using a Malvern Mastersizer 2000  
169 (Institute of Geography, University of Bern) on sub-samples collected at a 5-mm continuous  
170 interval. Before grain-size analysis, the samples were treated in a bath of diluted (30%)  
171 hydrogen peroxyde during 3 days to remove organic matter. After treatment, microscopic  
172 observations were performed to control that organic matter was totally dissolved. These grain-  
173 size analyses of the detrital material were performed to characterize event layers and, when  
174 event layers are induced by floods, to establish a proxy of flood intensity. Grain-size  
175 variability is assumed to be related with the stream flow energy of the river entering the lake  
176 and, thereby, with the peak discharge reached during the flood event (Campbell, 1998;  
177 Lapointe et al., 2012; Wilhelm et al., 2015). The flood intensity may also be reconstructed  
178 based on the amount of sediment transported and deposited during floods (e.g. Schiefer et al.,  
179 2011; Jenny et al., 2014; Wilhelm et al., 2015). This approach appears particularly relevant in  
180 case of an insignificant variability of the flood-sediment grain size (e.g. Jenny et al., 2014;  
181 Wilhelm et al., 2015). When the depositional pattern of the flood layers within the lake basin  
182 (assessed through the stratigraphic correlation) shows a high variability, many cores are  
183 required for a reliable assessment of the flood-sediment volumes (e.g. Page et al., 1994;  
184 Schiefer et al., 2011; Jenny et al., 2014). However, when the depositional pattern of the flood  
185 layers is stable over time, the layer thickness in one core may be sufficient (e.g. Wilhelm et  
186 al., 2012b; 2015). As a result, grain size and sediment volume of the event layers were both  
187 explored as two distinct proxies of flood intensity.

188

### 189 **3.3. Coprophilous fungal spores analysis**

190 Erosion processes in high-altitude catchments may be modified by grazing activity and,  
191 thereby, the climatic signal in flood reconstructions may be altered (e.g. Giguet-Covex et al.,  
192 2012). The variability of grazing intensity in a catchment area can be reconstructed from the

193 sedimentary abundance of coprophilous fungal ascospores, i.e. *Sporormiella* (HdV-113) (e.g.  
194 Davis and Schafer, 2006; Etienne et al., 2013). To test the potential impact of grazing  
195 intensity on the reconstructed flood activity, *Sporormiella* abundance was determined in  
196 subsamples collected all along the core FOR13P3 with an approximate step of 3 cm. This core  
197 was chosen because it was the sequence with the thinnest potentially-erosive event layers.  
198 During the sampling, event layers were avoided because they may correspond to layers  
199 induced by flood or mass-movement events that may have transported unusual quantities of  
200 *Sporormiella* ascospores, or induced the remobilization of older sediments. Subsamples were  
201 chemically prepared according to the procedure of Fægri and Iversen (1989). *Lycopodium*  
202 *clavatum* tablets were added in each subsample (Stockmarr, 1971) to express the results in  
203 concentrations (number.cm<sup>-3</sup>) and accumulation rates (number.cm<sup>2</sup>.yr<sup>-1</sup>). Coprophilous fungal  
204 ascospores were identified based on several catalogues (Van Geel and Aptroot, 2006; Van  
205 Geel et al., 2003) and counted following the procedure established by Etienne and Jouffroy-  
206 Bapicot (2014).

207

### 208 **3.4. Dating methods**

209 For dating the lake sequence over the last century, short-lived radionuclides (<sup>210</sup>Pb, <sup>137</sup>Cs)  
210 were measured by gamma spectrometry at the EAWAG (Zürich, Switzerland). The core  
211 FOR13P4 was sampled following a non-regular step of 1±0.2 cm. The non-regular step aims  
212 at matching the facies (i.e. sedimentary background or event layer) boundaries for  
213 homogeneous samples. The <sup>137</sup>Cs measurements allowed two main chronostratigraphic  
214 markers to be located: the fallout of <sup>137</sup>Cs from atmospheric nuclear weapon tests culminating  
215 in AD 1963 and the fallout of <sup>137</sup>Cs from the Chernobyl accident in AD 1986 (Appleby,  
216 1991). The decrease in excess <sup>210</sup>Pb and the Constant Flux/Constant Sedimentation (CFCS)  
217 allowed a mean sedimentation rate to be calculated (Goldberg, 1963). The standard error of  
218 the linear regression of the CFCS model was used to estimate the uncertainty of the  
219 sedimentation rate obtained by this method. The <sup>137</sup>Cs chronostratigraphic markers are then  
220 used to control the validity of the <sup>210</sup>Pb-based sedimentation rate.

221 To date the sequence beyond the last century, small-size vegetal macro-remains were sampled  
222 in core FOR13P4. Terrestrial plant remains were isolated at the Institute of Plant Sciences  
223 (University of Bern) and sent for AMS <sup>14</sup>C analysis to the AMS LARA Laboratory  
224 (University of Bern). <sup>14</sup>C ages were calibrated using the Intcal13 calibration curve (Reimer et



225 al., 2013; Table 1). In addition, palaeomagnetic chronostratigraphic markers were also used.  
226 These markers can be obtained by comparing the characteristic declination and inclination of  
227 remanent magnetization (ChRM) versus depth to global geomagnetic models or to known  
228 secular variations of the geomagnetic field (e.g. Barletta et al., 2010; Wilhelm et al., 2012a).  
229 Palaeomagnetic investigations were performed at the CEREGE laboratory (University Aix-  
230 Marseille) and are detailed in supplementary material.

231 Using the R-code package “clam” (Blaauw, 2010), an age-depth model was generated from  
232 the  $^{210}\text{Pb}$  ages, the  $^{14}\text{C}$  ages and the palaeomagnetic chronological markers.

233

## 234 **4. Results**

235

### 236 **4.1. Sedimentology**

237 The sediment consists of a homogeneous, brown mud mainly composed of silty detrital  
238 material and aquatic organic remains (small fragments of plants and amorphous organic  
239 matter), representing the background hemi-pelagic sedimentation. These fine grained deposits  
240 are interrupted by 171 rather coarser-grained layers, which are interpreted to represent short-  
241 term depositional events, i.e. event layers (Fig. 2).

242 The 171 event layers correspond to graded layers, characterized by their higher density, a  
243 slight fining-upward trend and a thin, whitish fine-grained capping layer (Fig. 2). There is no  
244 evidence of an erosive base. According to the stratigraphic correlation, almost all these graded  
245 layers (168 out of 171) extend over the entire lake basin with a regular deposition pattern. The  
246 thickness of these 168 graded layers is systematically larger in cores FOR13P2 and FOR13P4,  
247 and decreases respectively in cores FOR13P1 and FOR13P3. This suggests that the southern  
248 branch of the Bouchouse stream is the main sediment input over the studied period (Fig. 1).  
249 The grain-size of these graded layers is dominated by silt-sized grains with only small  
250 amounts of clay / fine silt present in the whitish capping layer and to coarse silt in their basal  
251 part (Fig. 2 and S1). The origin of these 168 is discussed in section 5.1. The three other  
252 graded layers show a higher variability in thickness, grain size and depositional pattern.  
253 Above all, they overlie three cm-thick coarse-grained layers, present at 75 cm in core  
254 FOR13P2 and at 9 and 42 cm in core FOR13P4 (Fig. 2). The coarse-grained layers consist of  
255 pebble gravels and aquatic plant remains embedded in a silty matrix. The high porosity in the  
256 sediment due to the presence of gravels generates a partial loss of XRF signal, preventing a

257 reliable geochemical characterization. X-ray images show chaotic sedimentary structures. The  
258 stratigraphic correlation revealed that two centimetres of sediment are missing below the  
259 thickest coarse-grained layer in core FOR13P4, suggesting an erosive base for this layer. The  
260 stratigraphic succession of a coarse-grained layer overlain by a graded layer (labelled MMIL  
261 in Fig. 2 and 3) suggests that the two layers were induced by a single event. Their origin is  
262 discussed in section 5.1.

263

## 264 **4.2. Geochemistry**

265 Among the core scanner output parameters, the scattered incoherent (Compton) radiation of  
266 the X-ray tube ( $Mo_{inc}$ ) may vary with the sediment density (Croudace et al., 2006) and,  
267 thereby, offer a high-resolution proxy for sediment density.  $Mo_{inc}$  values were averaged at a  
268 5-mm resolution to be compared to the density obtained at a 5-mm resolution with the  
269 gamma-ray attenuation method. A positive and significant correlation ( $r=0.85$ ,  $p<10^{-4}$ )  
270 between the two density parameters was found and allowed using  $Mo_{inc}$  as a proxy of  
271 sediment density for identifying millimetre-scale event layers (Fig. 3).

272 The variability of other elements within the event layers was then investigated to assess i) a  
273 high-resolution grain-size proxy and ii) distinct sediment sources of the event layers between  
274 the littoral (i.e. mass-movement origin) and the catchment area (i.e. flood origin). The  
275 variability of potassium (K) intensities vs. sediment depth (Fig. 2 and S1) shows increased K  
276 intensities in the capping layers of the event layers, suggesting K enrichment in the finest  
277 sediment fraction. Variability in silicon (Si) intensities is correlated to K intensities ( $r=0.77$ ,  
278  $p<10^{-4}$ ). Variations in iron (Fe) intensities show an opposite pattern with Fe enrichments in  
279 the basal and coarser part of the graded beds. Interestingly, Fe is the only element which  
280 elevated in event layers. These results suggest that the Fe/K ratio may be used as a millimetre-  
281 scale proxy for relative grain-size distribution and hence for detecting millimetre-scale event  
282 layers. However, since grain-size variability is insignificant, the information that can be won  
283 from this proxy in regard to flood-intensity reconstruction is minor.

284 Ca intensities are most of the time very low ( $< 900$  counts), except for several sharp peaks and  
285 two well-marked excursions ( $> 1200$  counts) at 30 and 75 cm in core FOR13P2 (Fig. 3).  
286 These two well-marked excursions correspond to the two thickest graded layers (labelled  
287 MMIL2 and 3; Fig. 2). In addition, manganese (Mn) intensities also vary within a low value  
288 range ( $< 10^4$  counts) interrupted by sharp, well-marked peaks (up to  $4 \cdot 10^4$  counts). All those

289 Mn peaks are located at the base of the 168 graded layers (those that not overlain a coarse-  
290 grain layers). However not every base of graded layers corresponds to a Mn peak. To better  
291 assess the relationships between those elements, the Ca intensities were plotted against Fe, K  
292 and Mn intensities (Fig. 3). These plots clearly highlight two groups of deposits. The  
293 background sediments and the 168 graded layers (those labelled FIL in Fig. 3) are  
294 characterized by i) low Ca intensities and ii) a high variability in Mn intensities. The three  
295 graded layers labelled MMIL in figure 2 show a distinct geochemical pattern with (i) high Ca  
296 intensities regardless of Fe and K intensities and (ii) very low Mn intensities.

297

### 298 **4.3. Chronology**

299 The down-core  $^{210}\text{Pb}$  excess profile for core FOR13P2 shows a continuous decrease to low  
300 values ( $\sim 50 \text{ Bq.Kg}^{-1}$ ), punctuated by sharp excursions to low values for three layers (2-3.5  
301 cm, 7.5-10.5 cm and 15-17 cm) corresponding to graded layers (Fig. 4A). In line with Arnaud  
302 et al. (2002), these values were excluded to build a corrected sedimentary record without  
303 event layers (Fig. 4B). The CFCS model (Goldberg, 1963), applied on the event-free  $^{210}\text{Pb}$   
304 excess profile, provides a mean sedimentation rate of  $1.3 \pm 0.1 \text{ mm.yr}^{-1}$  (without the event  
305 layers). Ages derived from the CFCS model were transposed to the original sediment  
306 sequence to provide a continuous age-depth relationship (Fig. 4C). The event-free  $^{137}\text{Cs}$   
307 profile indicated two peaks at 3.5 cm and 5.5 cm (Fig. 4B), interpreted as the result of the  
308 Chernobyl accident in AD 1986 and the maximum fallout of the nuclear weapon tests in AD  
309 1963. These independent chronological markers are in good agreement with the  $^{210}\text{Pb}$  excess  
310 ages, supporting the age-depth model over the last century (Fig. 4C).

311 In order to evaluate the reliability and efficiency of the palaeomagnetic results several points  
312 need to be verified: i) the preservation of the sedimentary magnetic fabric, ii) the stability of  
313 magnetic mineralogy, and iii) the stability of the magnetic components. Results of Anisotropy  
314 of Magnetic Susceptibility for core FOR13P4 show a well preserved sedimentary fabric, i.e.  
315  $K_{\text{min}}$  inclination close to the vertical, except in the thickest event layers (labelled MMIL2  
316 and MMIL3, Fig. 2) where the  $K_{\text{min}}$  inclination is clearly deviated (Fig. S2). For the 3 cores,  
317 the mean destructive field of ARM and IRM is very similar (between 20 and 30 mT)  
318 indicating a magnetic mineralogy mainly composed of low coercivity phase. The S-ratio  
319 (Bloemendal et al., 1992) is always between 0,86 and 0,95 indicating lower coercivity and a  
320 ferrimagnetic mineralogy. This suggests a good stability of the magnetic mineralogy, except

321 in event layers where other parameters such as the relative palaeointensity (calculated as  
322 NRM intensity divided by ARM intensity) are clearly different, highlighting a different  
323 magnetic mineralogy. PCA have then been performed using puffin plot software (Lurcock  
324 and Wilson, 2012) to calculate the ChRM. A careful examination of demagnetization  
325 diagrams shows a unidirectional behaviour (Fig. S3). The Mean Angular Deviation (MAD) is  
326 usually lower than 6 revealing a good stability of the magnetization direction. In most cases,  
327 the calculated component is not straight to the origin. This is particularly the case in the event  
328 layers. This implies the occurrence of a high coercivity component of unknown origin. All  
329 cores show quite large variations of the declination and inclination *vs.* depth. Because of the  
330 deviation of the Kmin and changes in magnetic mineralogy, measurements from the thickest  
331 event layers (i.e. MMIT2 and MMIT3) have been removed to build event-free declination and  
332 inclination signals (Fig. 5A). Based on the stratigraphic correlation, the event-free  
333 palaeomagnetic profiles obtained for each core were all corrected to a reference depth, i.e. the  
334 event-free depth of core FOR13P2 (Fig. 5B). Finally, all magnetic profiles were averaged to  
335 obtain unique curves of declination *vs.* depth and inclination *vs.* depth (Fig. 5C), smoothing  
336 small artefacts and making it easier for comparison to the reference curve (ARCH3.4k model;  
337 Donadini et al., 2009; Korte et al., 2009). From the variations of the reference curve over the  
338 last millennium, magnetic declination minima and maxima can be identified at AD 1810  $\pm$ 20,  
339 1540  $\pm$ 70 and 1365  $\pm$ 25 (D-1 to D-3, respectively). For the inclination, two tie points at AD  
340 1700  $\pm$ 30 and 1330  $\pm$ 40 can be used (I-1 and I-2, Fig. 5D). Furthermore the ChRM  
341 declination profile presents 3 declination features and the ChRM inclination profile presents 2  
342 inclination features over this period, allowing the correlation proposed (Fig. 5). These well-  
343 correlated declination and inclination features can thus be used as additional chronological  
344 markers.

345 The  $^{210}\text{Pb}$  and the  $^{14}\text{C}$  ages (Fig. 4 and Table 1) were then combined with the palaeomagnetic  
346 chronomarkers (Fig. 5) to construct an age-depth model covering the whole sequence (Fig. 6).  
347 As noted above, the age-depth model was calculated on an event-free depth using a smooth  
348 spline with the “clam” R-code package (Blaauw, 2010). This revealed that the sequence FOR  
349 covers the last millennium with a mean sedimentation rate of 1 mm.yr<sup>-1</sup> (without event  
350 layers).

351

## 352 **5. Discussion**

353

### 354 **5.1. Different triggers for event layers**

355

#### 356 **5.1.1. Mass movements**

357 The unusual presence of gravel and aquatic plant remains, in combination with the chaotic  
358 sedimentary structures and the localized deposition areas, suggest that the coarse-grained  
359 layers result of a mass movement originating from sediment-charged slopes (e.g. Sauerbrey et  
360 al., 2013). The three graded layers overlying the coarse-grained layers are then resulting from  
361 the sediment that is transported in suspension during sliding of subaquatic slope sediments  
362 and then deposited over the coarse-grained layers and further into the lake basin (e.g.  
363 Girardclos et al., 2007; Moernaut et al., 2014). As a result, each stratigraphic succession of a  
364 graded and a coarse-grained layer is interpreted as a mass-movement-induced layer (MMIL).  
365 These MMILs are well characterized by higher Ca intensities that suggest a distinctly  
366 different sediment source when compared to the sedimentary background and to the 168  
367 graded layers that not overlain a coarse-grain layer. The coarse-grained layer of MMIL3 is  
368 only present in core FOR13P3, suggesting a littoral origin of the mass movement (Fig. 2). The  
369 two coarse-grained layers of MMIL1 and MMIL2 are located in core FOR13P4 (Fig. 2).  
370 These layers may thus originate either from the delta or from the littoral slopes. Slope angles  
371 of  $< 10^\circ$  and  $\sim 15^\circ$  for delta and littoral slopes of Lake Foréant, respectively, point to a littoral  
372 origin as suggested by many studies showing that slope angles  $> 10^\circ$  are favourable for the  
373 generation of mass-movements (e.g. Moernaut et al., 2007; Strasser et al., 2011; Van Daele et  
374 al., 2013). In addition, higher Ca intensities are often an indicator of littoral sediments as a  
375 result of increased fluxes of endogenic calcite when compared to the open-water endogenic  
376 production.

377

#### 378 **5.1.2. Flood events**

379 The 168 graded layers may be induced by either mass movements or flood events (e.g. Sturm  
380 and Matter, 1978). Their extents over the whole basin with a relatively homogeneous  
381 deposition pattern, their frequent occurrence and a different geochemical pattern suggest a  
382 distinct origin from that of the MMIL graded layers. The low Ca intensities suggest a minor

383 sediment contribution of the marble and calc-schists in favour of a major contribution of the  
384 arkose band, which is the lithology drained by the main inflow (Fig. 1). The 168 graded layers  
385 are also characterized by sharp peaks of Mn only located at their bases. This location suggests  
386 that the punctual enrichment in Mn is related to the occurrence of these event layers. Mn is a  
387 redox sensitive element and more soluble under reducing conditions (e.g. Davison, 1993;  
388 Torres et al., 2014). The punctual presence of detectable Mn at the base of the graded layers  
389 suggests that hyperpycnal turbidity currents carry oxygen to the deeper parts of the basin.  
390 Dissolved oxygen is probably also trapped in pore waters of the individual graded layers.  
391 Based on these considerations we suggest that dissolved and reduced Mn is, in part due to the  
392 rapid increase in loading from the graded layers, migrating from pore waters of the buried  
393 sediments into oxygenated graded layers where it is oxidized and precipitated likely in form  
394 of an Mn-oxyhydroxide (e.g. Davison, 1993; Deflandre et al., 2002). The fast sediment  
395 deposition during the event-layer formation and the low reactive organic matter  
396 concentrations would then prevent reductive dissolution of the Mn-oxyhydrxide precipitates  
397 (e.g. Torres et al., 2014). According to these layer characteristics, flood events are the most  
398 probable candidate to trigger the 168 graded layers because i) these events may be frequent  
399 (e.g. Czymzik et al., 2013), ii) these events may bring both high oxygen and detrital inputs in  
400 a short time (e.g. Deflandre et al., 2002), and iii) the nature of the sediment correspond the  
401 most to the main lithology drained by the inflow. Hence, the 168 graded layers likely  
402 correspond to flood-induced layers (FIL).

403

### 404 **5.1.3. Chronological controls**

405 MMILs can be triggered by spontaneous failures due to overloading/oversteepening of  
406 sediments-charged slopes, snow avalanches, rockfalls, earthquakes or fluctuations in lake  
407 levels (e.g. Monecke et al., 2004; Girardclos et al., 2007; Moernaut et al., 2014). In case of  
408 Lake Foréant, changes in lake level can be excluded because water levels of Lake Foréant are  
409 well controlled by bedrock outlets. In addition, there is no geomorphological evidence of  
410 major rockfalls in the catchment area. Regarding earthquakes, many events occurred in the  
411 region and affected the population and infrastructure. Historical earthquakes are well  
412 documented thanks to the database SisFrance (<http://www.sisfrance.net>, Lambert and Levret-  
413 Albaret, 1996; Scotti et al., 2004). An earthquake trigger for the MMILs can then be  
414 investigated by comparing ages of the MMILs to the dates of the closest and/or strongest  
415 historical earthquakes (e.g. Avşar et al., 2014; Howarth et al., 2014). The three MMILs are

416 respectively dated to AD 1963 ( $\pm 6$ ), AD 1814 (+50/-39) and AD 1456 (+19/-56) (Fig. 6). The  
417 age of the most recent deposit is consistent with the Saint-Paul-sur-Ubaye earthquake (AD  
418 1959), characterized by an epicentre at ca. 20 km from the lake where the MSK intensity  
419 reached VII-VIII. The age of the second deposit is consistent with the Piemont (Torre Pellice)  
420 earthquake (AD 1808), characterized by an epicentre at ca. 20 km from the lake and a MSK  
421 intensity of VIII (Fig. 6). For the older period of the third deposit, data of documented  
422 earthquakes are sparser in the catalogue, precluding a reliable assignment. The earthquakes of  
423 Saint-Paul-sur-Ubaye and Piemont are both the closest and strongest historically-known  
424 earthquakes around the lake, suggesting that they are the most probable trigger of the  
425 temporarily corresponding subaquatic landslides. Overall, there is a good agreement between  
426 major historical events and the calculated ages of the MMILs supporting their sedimentologic  
427 interpretation and the chronology over the last centuries.

428

## 429 **5.2. Palaeoflood record**

430 A flood chronicle of the Bouchouse stream was built by dating the 168 FILs over the last  
431 millennium. Changes in flood frequency are highlighted through a running sum of flood  
432 occurrences with an 11-year (Fig. 7) or 31-year window (Fig. 8). The absence of significant  
433 grain-size variability precludes the use of grain size to assess changes in flood intensity (e.g.  
434 Giguët-Covex et al., 2012; Lapointe et al. 2012; Wilhelm et al., 2013, 2015). The relatively  
435 homogeneous grain size of the FILs makes the sediment accumulation per event a more  
436 suitable proxy of flood intensity (e.g. Jenny et al., 2014). In addition, the relatively  
437 homogeneous flood-sediment deposition pattern within the lake basin makes it possible to use  
438 the FIL thickness as a proxy of the flood-sediment accumulation as shown by previous  
439 calibration in Alpine environments (Wilhelm et al., 2012b; Jenny et al., 2014; Wilhelm et al.,  
440 2015). Hence, the FIL thickness is here assumed to represent the flood intensity, under the  
441 condition that erosion processes and availability of erodible materials in the catchment did not  
442 change significantly over time.

443

### 444 **5.2.1. Proxy validation**

445 To control the reliability of our reconstruction, the Foréant palaeoflood record is compared to  
446 the historical floods at Ristolas located around 8 km downstream the lake (Fig. 1C and  
447 Supplementary Material). The almost absence of documented flood event for the Bouchouse

448 stream (outlet of Lake Foréant) precludes an event-to-event comparison as undertaken with  
449 the Lake Allos record (Wilhelm et al., 2015). Hence, the 21 flood events having affected the  
450 village of Ristolas and occurring during the ice-free season of the lake (mid-June to mid-  
451 November) have been considered to reconstruct a historical flood record (Fig. 7). This  
452 includes 6 floods considered as 'local' because they only affected the village of Ristolas  
453 (catchment area of ca. 80 km<sup>2</sup>) and 15 floods considered as 'sub-regional' because they also  
454 affected other villages downstream (Abriès, Aiguilles, Chateau-Vieille-Ville, catchment area  
455 of ~320 km<sup>2</sup>). Through comparison of the historical chronicles and the lake records, we  
456 observe that the ranges of flood-frequency values are similar, i.e. between 0 and around 4  
457 floods per 11 years. We also observe strong similarities in the two flood records with common  
458 periods of low flood frequency in AD 1750-1785, 1820-1860 and 1910-1945 and common  
459 periods of high flood frequency in AD 1785-1820, AD 1945-1970 and AD 1985-2000. Only a  
460 slight time lag (~5 years) appears for the latter period in the lake record. Overall, there is then  
461 good agreement with the historical data, supporting that Lake Foréant sediments record the  
462 variability of past flood events that impacted societies over the last 250 years relatively well.  
463 A major inconsistency, however, appears from 1860 to 1910 since numerous floods are  
464 documented in the lake record but there is missing evidence for flood in the historical record.  
465 A high hydrological activity is documented for the region at this time (e.g. Miramont et al.,  
466 1998; Sivan et al., 2010; Wilhelm et al., 2012a; 2015), suggesting that this may result of a  
467 historical database locally incomplete.

468

### 469 **5.2.2. Potential influences of environmental changes**

470 The Foréant flood record may be considered as relevant over the entire studied period if  
471 erosion processes are stable over time. Erosion processes in the Foréant catchment may be  
472 affected by modifications in the river system and/or by land-use changes.

473 The main inflow, the Bouchouse stream, has built an alluvial plain upstream the lake where it  
474 is divided in two main meandering branches. An alternate activity of these branches during  
475 floods may disturb the flood record by triggering variable sediment dispersion within the lake  
476 basin (e.g. Wilhelm et al., 2015). However, such processes seem to be unlikely because the  
477 stratigraphic correlation highlights a stable pattern of the flood-sediment deposition with the  
478 thickest FILs in cores FOR13P2 and FOR13P4 from the depocenter and a thinning of the FIL  
479 deposits toward cores FOR13P1 and FOR13P3 located in the slopes (Fig. 2). The alluvial



480 plain may also disturb the record by acting as a sediment trap. Indeed, the meandering river  
481 morphology and the gentle slope of the alluvial plain may trigger a decrease of the discharge  
482 velocity, resulting in the deposition of the coarser particles on the plain before entering the  
483 lake. This may explain the small variability in grain-size in the Foréant sediment record. The  
484 grain-size ratio between the base (coarser fraction) and the top (finer fraction) of the FILs is  
485 ~1.3, while it usually ranges from 5 to 15 in many different geological and environmental  
486 settings (e.g. Oslegger et al., 2009; Giguët-Covex et al., 2012; Simmoneau et al., 2013;  
487 Wilhelm et al., 2013 Amman et al., 2015; Wilhelm et al., 2015). However, fine particles (i.e.  
488 clays and fine silts that composed the FILs) are transported by suspension in the river (e.g.  
489 Passega, 1964). As a result, their trapping and storage in the alluvial plain is unlikely. A  
490 negligible storage effect on the fine fraction is also supported by the relatively stable  
491 sedimentation rate of the silty sedimentary background (Fig. 6) that suggests an uninterrupted  
492 sediment transport to the lake over the studied period.

493 Erosion processes in the catchment may also be modified by land-use that mainly corresponds  
494 at this altitude to changes in grazing intensity. An increase of grazing intensity may make  
495 soils more vulnerable to erosion during heavy rainfalls and, thereby, may induce an increased  
496 sensitivity of the catchment-lake system to record floods, i.e. higher flood frequency and/or  
497 flood-sediment accumulation in the sediment record (e.g. Giguët-Covex et al., 2012).  
498 Abundance of *Sporormiella* is assumed to reflect local changes of grazing intensity in Lake  
499 Foréant catchment (e.g. Etienne et al., 2013). The concentration of *Sporormiella* ascospores  
500 measured in core FOR13P3 oscillated from 5 to 43 number.cm<sup>-3</sup> through the sequence (Fig.  
501 2), resulting in accumulation rates varying from 12 to 340 number.cm<sup>2</sup>.yr<sup>-1</sup> over time (Fig. 8).  
502 This variability in *Sporormiella* abundance has been compared to the variability in flood  
503 frequency and flood-sediment accumulation (see Supplementary Material). We do not find  
504 significant relationships ( $p > 0.05$ ) between these parameters (Fig. S4), suggesting that  
505 variations in pastoralism seemingly have not had a significant impact on erosion processes in  
506 the Foréant catchment. However, two samples covering the period AD 1734-1760 show both  
507 high *Sporormiella* accumulation rates and flood frequencies (Fig. 8 and S3). This suggests  
508 that the flood frequency during this period may be exacerbated by a punctual and very high  
509 grazing intensity. Hence, we postulate that erosion processes did not change drastically over  
510 the studied period, implying that climate is likely the main factor explaining the recorded  
511 flood activity, with exception of the period AD 1734-1760.

512

### 513 **5.2.3. Palaeoflood activity in the regional climatic setting**

514 Comparison with the historical record shows that the past flood variability is well reproduced  
515 by the Foréant record (Fig. 7). The Foréant palaeoflood record is thus interpreted as the  
516 recurrence of summer-to-autumn flood events triggered by both local and mesoscale  
517 convective phenomena.

518 To discuss the millennium-long flood variability in regard to both Atlantic and Mediterranean  
519 climatic influences in the Alpine domain, the Foréant palaeoflood record is compared to the  
520 palaeoflood records of Lakes Blanc and Allos (Fig. 7 and 8). Lakes Blanc and Allos have  
521 similar characteristics to Lake Foréant such as the high altitude (> 2000 m a.s.l.), the small  
522 catchment area (< 3 km<sup>2</sup>) and the steep catchment slopes, making possible the comparison.  
523 Lake Blanc sediments located in the northern French Alps mainly record Atlantic-sourced  
524 weather pattern of high altitude, i.e. summer local convective events (Fig. 1; Giguet-Covex et  
525 al., 2012; Wilhelm et al., 2012b, 2013). In contrast, Lake Allos sediments located in the  
526 southern French Alps mainly record Mediterranean-sourced weather patterns of high altitude,  
527 i.e. mesoscale convective events (Fig. 1; Wilhelm et al., 2012a, 2015). The last millennium is  
528 usually divided in three climatic periods according to the temperature variations; the warm  
529 Medieval Climate Anomaly (MCA, ca. AD 950-1250), the cold Little Ice Age (LIA, ca. AD  
530 1300-1900) and the warmer 20<sup>th</sup> century (e.g. Lamb, 1965; Büntgen et al., 2011; Luterbacher  
531 et al., 2012 and references therein). During the MCA, the Foréant flood record shows a low  
532 flood frequency with ~10 floods per century and, 4 occurrences of thick flood deposits (> 8  
533 mm thick) that we interpret as high-intensity flood events. During the LIA, the Foréant record  
534 shows a higher flood frequency with ~17 floods per century and only 2 high-intensity events.  
535 The 20<sup>th</sup> century is finally characterized by ~17 floods per century and absence of high-  
536 intensity events. The increased flood frequency during the long and cold period of the LIA,  
537 compared to the MCA, was also observed in the Blanc and Allos records (Wilhelm et al.,  
538 2012a; 2013; Fig. 8), as well as in many other records from the European Alps (e.g. Arnaud et  
539 al., 2012; Glur et al., 2013; Swierczynski et al., 2013; Wirth et al., 2013a, 2013b; Amann et  
540 al., 2015; Schulte et al., 2015) and the north-western Mediterranean area (e.g. Jorda and  
541 Provansal, 1996; Camuffo and Enzi, 1995; Jorda et al., 2002; Thorndycraft and Benito, 2006;  
542 Moreno et al., 2008; Benito et al., 2015; Arnaud-Fassetta et al., 2010). This common pattern  
543 in many flood records of southern Europe may be the result of a southward shift and an  
544 intensification of the dominant westerly winds during boreal summer related to an increase in  
545 the thermal gradient between low (warming) and high (cooling) latitudes (e.g. Bengtsson and

546 Hodges, 2006; Raible et al., 2007). In this scenario, the Alps are likely to experience an  
547 increase in precipitation due to an increase in moisture advection from the North Atlantic. In  
548 contrary, the occurrence of high-intense floods during both the MCA and the LIA periods is a  
549 new feature of Alpine regional patterns, since the most intense floods occurred exclusively  
550 during the MCA in the Blanc record (Wilhelm et al., 2013) or during the LIA in the Allos  
551 record (Wilhelm et al., 2012a; Fig. 8) and other Mediterranean records of the Alpine region  
552 (Jorda and Provansal, 1996; Miramont et al., 1998; Jorda et al., 2002; Arnaud-Fassetta et al.,  
553 2010). This suggests that hydro-meteorological processes related to the Atlantic and to the  
554 Mediterranean climatic influences may alternatively trigger high intense events in the Foréant  
555 area during the MCA and the LIA, respectively. However, the most intense floods at Foréant  
556 appear 3 times more frequent during the MCA than during the LIA, a trend that remains true  
557 when considering various thickness thresholds (8, 7, 6 or 5 mm) for high-intensity flood  
558 events. In addition, the mean sediment accumulation per flood event shows values ~50%  
559 higher during the MCA than during the LIA (3.8 vs. 2.4 mm/flood), suggesting an increase of  
560 the mean flood-event intensity during the warmer period. These two evidences of increased  
561 flood intensity during the warm period may be related to the strengthening of local convective  
562 processes due to higher temperatures, as suggested for the north-western flood pattern  
563 (Giguet-Covex et al., 2012; Wilhelm et al., 2012b, 2013). In the Foréant area, higher  
564 temperatures seem thus to result in a lower flood frequency but in higher flood intensity on  
565 the multi-centennial time scale. Flood frequency and intensity during the warmer 20<sup>th</sup> century,  
566 however, do not follow these trends. The frequency is still similar to the LIA one and high-  
567 intense events are absent and the mean sediment accumulation per flood event (2.2 mm/flood)  
568 is also similar to the LIA. Two hypotheses may be considered to explain this ‘anomaly’. First,  
569 this may result from the relatively short period covered by the 20<sup>th</sup> century (i.e. ~100 years) in  
570 comparison with the multi-centennial variability documented for the MCA (i.e. ~300 years)  
571 and the LIA (i.e. ~600 years) periods. Thereby, considering stable temperature-flood  
572 relationships over time, the 20<sup>th</sup> century might be a transitional period toward a MCA-like  
573 flood pattern with the global warming. This latter possibility would imply an increasing flood  
574 hazard in the Foréant region in a near future due to an increased occurrence of high-intensity  
575 flood events. Secondly, this may also result from a non-linearity of the flood response to  
576 temperature, making the analogy between the MCA and the 20<sup>th</sup> century more complex, in  
577 particular as the current warming is caused by an unprecedented forcing (greenhouse gases).  
578 Moreover, the other external forcing such as solar activity, and volcanic eruptions largely  
579 varied over the last millennium (e.g. Servonnat et al., 2010; Delaygue et Bard, 2011; Gao et

580 al., 2012; Crowley and Unterman, 2013) and their non-linear combination also with the  
581 greenhouse gases may result in different time-space temperature patterns and, thereby, in  
582 different flood responses during these two periods. In order to explore forcing-dependent  
583 impacts on the climate-flood relationships, deeper analysis utilizing for example advanced  
584 statistics or simulations is required.

585

## 586 **6. Conclusion**

587 High-resolution sedimentological and geochemical analyses of the Lake Foréant sequence  
588 revealed 171 event layers. Three of the 171 event layers can be differentiated by characteristic  
589 geochemical features (high Ca contents and low Mn contents) and stratigraphic succession.  
590 These three event layers are interpreted as mass-movement-induced layers. The other 168  
591 event layers show a geochemical pattern similar to the sedimentary background that mainly  
592 corresponds to detrital material sourced by the rivers. These event layers are interpreted as  
593 flood-induced layers. Only small changes in grain-size variability in the flood-induced layers  
594 precluded the use of the grain size as a flood-intensity proxy. However, the relatively  
595 homogeneous grain size and deposition pattern within the lake basin made the flood-deposit  
596 thickness a suitable proxy for the reconstruction of flood intensity.

597 Comparison with local historical data indicates that Foréant sediments sensitively record past  
598 flood events with variability in frequency and intensity related to both Atlantic- and  
599 Mediterranean-influenced hydro-meteorological processes, i.e. local and mesoscale  
600 convective systems occurring from late spring to fall. As there is no evidence of major  
601 changes in erosion processes due to landscape evolution or grazing intensity (except maybe  
602 for the period AD 1734-1760), we assume that climate and not land-use changes exerts the  
603 dominant control on flood variability in the Foréant-record over the past millennium. The  
604 comparison to northern and southern flood records, i.e. to Atlantic- and Mediterranean-  
605 influenced records, highlights that the increase of flood frequency during the cold period of  
606 the LIA is a common feature of all regional flood patterns from the European Alps. The  
607 comparison also revealed that high-intensity events in the Foréant region occurred during both  
608 the cold LIA and the warm MCA periods. This specific feature of the Foréant flood record  
609 likely results from its sensitivity to both Atlantic and Mediterranean climatic influences.  
610 However, high-intensity events are more frequent and the flood intensity is higher during the  
611 warm MCA. This suggests that flood hazard may increase in the Foréant region in response to

612 global warming. Surprisingly, the flood variability over the warm 20<sup>th</sup> century appears still  
613 similar to the flood variability of the cold LIA period. This 20<sup>th</sup>-century flood trend may be  
614 interpreted as the result of a transitional period toward a MCA-like flood pattern. This would  
615 imply an increasing flood hazard in the Foréant region in a near future due to more frequent  
616 high-intensity flood events. However, this may also result from a non-linear temperature-  
617 flood relationship. In order to better understand the underlying mechanisms deeper analyses  
618 employing advanced statistics or simulations need to be applied.

619

## 620 **Acknowledgments**

621 B. Wilhelm's post-doctoral fellowship (2013-2014) was supported by a grant from the AXA  
622 Research Fund. We would also like to thank Pierre Sabatier for his help with analysis of the  
623 <sup>210</sup>Pb data, Anne-Lise Develle for fruitful discussions, Petra Boltshauser-Kaltenrieder for help  
624 with identification of terrestrial-plant remains prior to <sup>14</sup>C dating and Nicolas Thouveny and  
625 François Demory for providing access to facilities at the CEREGE palaeomagnetic laboratory  
626 (Aix-Marseille University) and for fruitful discussions.

627

628

629

## 630 **References**

631 Amann, B., Sönke, S., Grosjean, M.: A millennial-long record of warm season precipitation  
632 and flood frequency for the North-western Alps inferred from varved lake sediments:  
633 implications for the future, *Quaternary Science Reviews*, 115, 89-100, 2015.

634 Appleby, P.G., Richardson, N., Nolan, P.J.: <sup>241</sup>Am dating of lake sediments, *Hydrobiologia*,  
635 214, 35–42, 1991.

636 Arnaud, F., Lignier, V., Revel, M., Desmet, M., Pourchet, M., Beck, C., Charlet, F.,  
637 Trentesaux, A., Tribovillard, N.: Flood and earthquake disturbance of <sup>210</sup>Pb geochronology  
638 (Lake Anterne, North French Alps), *Terra Nova*, 14, 225–232, 2002.

639 Arnaud, F., Révillon, S., Debret, M., Revel, M., Chapron, E., Jacob, J., Giguex-Covex, C.,  
640 Poulénard, J., Magny, M.: Lake Bourget regional erosion patterns reconstruction reveals

641 Holocene NW European Alps soil evolution and paleohydrology, *Quaternary Science*  
642 *Reviews*, 51, 81–92, 2012.

643 Arnaud-Fassetta, G., and Fort, M.: Respective parts of hydroclimatic and anthropic factors in  
644 the recent evolution (1956-2000) of the active channel of the Upper Guil, Queyras, Southern  
645 French Alps, *Méditerranée*, 102, 143-156, 2004.

646 Arnaud-Fassetta, G., Carcaud, N., Castanet, C. and Salvador, P.G.: Fluvial  
647 palaeoenvironments in archaeological context: geographical position, methodological  
648 approach and global change—hydrological risk issues, *Quat. Int.*, 216, 93–117, 2010.

649 Avşar, U., Hubert-Ferrari, A., De Batist, M., Lepoint, G., Schmidt S. and Fagel N.:  
650 Seismically-triggered organic-rich layers in recent sediments from Göllüköy Lake (North  
651 Anatolian Fault, Turkey), *Quat. Sci. Rev.*, 103, 67–80, 2014.

652 Barletta, F., St-Onge, G., Channell, J.E.T. and Rochon, A.: Dating of Holocene western  
653 Canadian Arctic sediments by matching paleomagnetic secular variation to a geomagnetic  
654 field model, *Quaternary Science Reviews*, 29, 2315–2324, 2010.

655 Bengtsson, L., and Hodges, K.I.: Storm tracks and climate change, *Journal of Climate*, 19,  
656 3518–3543, 2006.

657 Beniston, M. and Stephenson, D.B.: Extreme climatic events and their evolution under  
658 changing climatic conditions, *Glob Planet Change*, 44, 1–9, 2004.

659 Benito, G., Macklin, M.G., Zielhofer, C., Jones A., and Machado, M.J.: Holocene flooding  
660 and climate change in the Mediterranean, *Catena*, 130, 13-33, 2015.

661 Blaauw, M.: Methods and code for ‘classical’ age modelling of radiocarbon sequences, *Quat.*  
662 *Geochronol.*, 5, 512–518, 2010.

663 Bloemendal, J., King, J.W., Hall, F.R. and Doh, S.-J.: Rock magnetism of Late Neogene and  
664 Pleistocene deep-sea sediments relationship to sediment source, diagenetic processes, and  
665 sediment lithology, *Journal of Geophysical Research*, 97: 4361-4375, 1992.

666 Boudevillain, B., Argence, S., Claud, C., Ducrocq, V., Joly, B., Lambert, D., Nuissier, O.,  
667 Plu, M., Ricard, D., Arbogast, P., Berne, A., Chaboureaud, J.P., Chapon, B., Crepin, F.,  
668 Delrieu, G., Doerflinger, E., Funatsu, B.M., Kirstetter, P.E., Masson, F., Maynard, K.,  
669 Richard, E., Sanchez, E., Terray, L. and Walpersdorf, A.: Cyclogenesis et précipitations  
670 intenses en région méditerranéenne: origines et caractéristiques, *La Meteorol.*, 66, 18–28,  
671 2009.

672 Boroneant, C., Plaut, G., Giorgi, F. and Bi., X.: Extreme precipitation over the Maritime Alps  
673 and associated weather regimes simulated by a regional climate model: Present-day and future  
674 climate scenarios, *Theor. Appl. Climatol.*, 86, 81–99, 2006.

675 Büntgen, U., Tegel, W., Nicolussi, K., McCormick, M., Frank, D., Trouet, V., Kaplan, J.,  
676 Herzig, F., Heussner, U., Wanner, H., Luterbacher, J., Esper, J. : 2500 years of European  
677 climate variability and human susceptibility, *Science*, 331, 578-582, 2011

678 Buzzi, A. and Foschini, L.: Mesoscale meteorological features associated with heavy  
679 precipitation in the Southern Alpine Region, *Meteorol. Atmos. Phys.*, 72, 131–146, 2000.

680 Campbell, C.: Late Holocene lake sedimentology and climate change in southern Alberta,  
681 Canada, *Quatern. Res.*, 49, 96–101, 1998.

682 Camuffo, D. and Enzi, S.: The analysis of two bi-millenary series: Tiber and Po River Floods,  
683 In: Jones, P.D. Bradley, R.S. Jouzel, J. (Eds.), *Climatic Variations and Forcing Mechanisms*  
684 of the Last 2000 years, NATO ASI Series, Series I: Global Environmental Change, 41  
685 Springer, Stuttgart, 433–450, 1995.

686 Corella, J.P., Benito, G., Rodriguez-Lloveras, X., Brauer, A. and Valero-Garcès, B.L.:  
687 Annually-resolved lake record of extreme hydro-meteorological events since AD 1347 in NE  
688 Iberian Peninsula, *Quat. Sci. Rev.*, 93, 77-90, 2014.

689 Croudace, I.W., Rindby, A. and Rothwell, R.G.: ITRAX: description and evaluation of a new  
690 multi-function X-ray core scanner. In: Rothwell, R.G. (Ed.), *New Techniques in Sediment*  
691 *Core Analysis*, Geological Society, London, Special Publications, 367, 51-63, 2006.

692 Crowley, T.J. and Untermann, M.B.: Technical details concerning development of a 1200-yr  
693 proxy index for global volcanism, *Earth Syst. Sci. Data*, 5, 187-197, 2013.

694 Cuvén, S., Francus, P. and Lamoureux, S.: Estimation of grain size variability with micro X-  
695 ray fluorescence in laminated lacustrine sediments, Cape Bounty, Canadian High Arctic,  
696 *Journal of Paleolimnology*, 44, 803–817, 2010.

697 Czymzik, M., Brauer, A., Dulski, P., Plessen, B., Naumann, R., von Grafenstein, U. and  
698 Scheffler, R.: Orbital and solar forcing of shifts in Mid- to Late Holocene flood intensity from  
699 varved sediments of pre-alpine Lake Ammersee (southern Germany), *Quatern. Sci. Rev.*, 61,  
700 96–110, 2013.

701 Davis, O.K. and Schafer, D.: *Sporormiella* fungal spores, a palynological means of detecting  
702 herbivore density. *Palaeogeog., Palaeoclimatol., Palaeoecol.*, 237, 40–50, 2006.

703 Davison, W.: Iron and manganese in lakes, *Earth-Science Reviews*, 34, 119-163,1993

704 Deflandre, B., Mucci, A., Gagne, J.P., Guignard, C., Sundby, B.: Early diagenetic processes  
705 in coastal marine sediments disturbed by a catastrophic sedimentation event, *Geochimica et*  
706 *Cosmochimica Acta*, 66(14), 2547–2558, 2002.

707 Delaygue, G. and Bard, E.: An Antarctic view of Beryllium-10 and solar activity for the past  
708 millennium, *Climate Dynamics*, 36, 2201–2218, 2011.

709 Donadini, F., M. Korte, Constable C. G.: Geomagnetic field for 0–3 ka: 1. New data sets for  
710 global modeling, *Geochemistry Geophysics Geosystems (G3)*, 10, Q06007,  
711 doi:10.1029/2008GC002295, 2009.

712 Durant, Y., Laternser, M., Giraud, G., Etchevers, P., Lesaffre, B., Merindol, L.: Reanalysis of  
713 44 Yr of Climate in the French Alps (1958–2002): Methodology, Model Validation,  
714 Climatology, and Trends for Air Temperature and Precipitation, *J. Applied Meteorology and*  
715 *Climatology*, 48(3):429-449, 2009.

716 Etienne, D., Wilhelm, B., Sabatier, P., Reyss, J.L. and Arnaud, F.: Influence of sample  
717 location and livestock numbers on *Sporormiella* concentrations and accumulation rates in  
718 surface sediments of Lake Allos, French Alps, *J. Paleolimnol.*, 49, 117–127, 2013.

719 Etienne, D. and Jouffroy-Bapicot, I.: Optimal counting limit for fungal spore abundance  
720 estimation using *Sporormiella* as a case study. *Veget. Hist. Archaeobot*, 23, 743-749, 2014.

721 Faegri, K. and Iversen, J.: *Textbook of Pollen Analysis*. John Wiley & Sons, New York. 328,  
722 1989.

723 Frei, C., Schöll, R., Fukutome, S., Schmidli, J., Vidale, P.L.: Future change of precipitation  
724 extremes in Europe: Intercomparison of scenarios from regional climate models, *J. Geophys.*  
725 *Res. Atm.*, 111, D06105. doi:10.1029/2005JD005965, 2006.

726 Gao, C., Robock, A. and Ammann, C.: Volcanic forcing of climate over the past 1500 years:  
727 An improved ice core-based index for climate models, *J. Geophys. Res.*, 113, D23111, 2008.

728 Giguet-Covex, C., Arnaud, F., Enters, D., Poulénard, J., Millet, L., Francus, P., David, F.,  
729 Rey, P.J., Wilhelm, B. and Delannoy, J.J.: Frequency and intensity of high altitude floods  
730 over the last 3.5 ka in NW European Alps, *Quatern. Res.*, 77, 12–22, 2012.

731 Gilli, A., Anselmetti, F.S., Glur, L. and Wirth, S.B.: Lake sediments as archives of recurrence  
732 rates and intensities of past flood events, In: *Dating Torrential Processes on Fans and Cones –*



733 Methods and Their Application for Hazard and Risk Assessment (Eds M. Schneuwly-  
734 Bollschweiler, M. Stoffel and F. Rudolf-Miklau), *Adv. Global Change Res.* 47, 225–242,  
735 2012.

736 Girardclos, S., Schmidt, O.T., Sturm, M. , Ariztegui, D., Pugin A., and Anselmetti F.S.: The  
737 1996 AD delta collapse and large turbidite in Lake Brienz, *Marine Geology*, 24, 137–154,  
738 2007.

739 Glur, L., Wirth, S.B., B€untgen, U., Gilli, A., Haug, G.H., Schär, C., Beer, J. and Anselmetti,  
740 F.S., Frequent floods in the European Alps coincide with cooler periods of the past 2500  
741 years, *Sci. Rep.*, 3, 2770, 2013.

742 Goldberg, E.D.: *Geochronology with 210Pb Radioactive Dating*, IAEA, Vienna, 121–131.  
743 1963

744 Gottardi, F., Obled, C., Gailhard, J., Paquet, E.: Statistical reanalysis of precipitation fields  
745 based on ground network data and weather patterns: Application over French mountains, *J.*  
746 *Hydrology*, 432–433, 154–167, 2010.

747 Howarth, J.D., Fitzsimons, S.J., Norris, R.J. and Jacobsen, G.E.: Lake sediments record high  
748 intensity shaking that provides insight into the location and rupture length of large  
749 earthquakes on the Alpine Fault, New Zealand, *Earth and Planetary Science Letters*, 403,  
750 340–351, 2014.

751 IPCC: *The Physical Science Basis. Contribution of Working Group I to the Fifth Assessment*  
752 *Report of the Intergovernmental Panel on Climate Change* (Eds T.F. Stocker, D. Qin, G.-K.  
753 Plattner, M. Tignor, S.K. Allen, J. Boschung, A. Nauels, Y. Xia, V. Bex and P.M. Midgley).  
754 Cambridge University Press, Cambridge, United Kingdom and New York, NY, USA, 2013

755 Jorda, M. and Provansal, M.: Impact de l’anthropisation et du climat sur le detritisme en  
756 France du sud-est (Alpes du Sud et Provence), *Bulletin de la Societe Geologique de France*,  
757 167, 159–168 ,1996.

758 Jorda, M., Miramont, C., Rosique, T. and Sivan, O.: Evolution de l’hydrosysteme durancien  
759 (Alpes du Sud, France) depuis la fin du Pleniglaciaire superieur, In: Bravard, J.-P., Magny, M.  
760 (Eds.), *Les Fleuves ont une Histoire, Paleo-environnement des Rivieres et des lacs Francais*  
761 *depuis 15000 ans. Errance, Paris*, 239–249, 2002.

762 Jenny, J.-P., Wilhelm, B., Arnaud, F., Sabatier, P., Giguet-Covex, C., Mélo, A., Fanget, B.,  
763 Malet, E., Ployon, E. and Perga, M.E., A 4D sedimentological approach to reconstructing the

764 flood frequency and intensity of the Rhône River (Lake Bourget, NW European Alps), *J.*  
765 *Paleolimnol.*, 51, 469–483, 2014.

766 Kylander, M.E., Klaminder, J., Wohlfarth, B., Löwemark, L.: Geochemical responses to  
767 paleoclimatic changes in southern Sweden since the late glacial: the Hässeldala Port lake  
768 sediment record, *J. Paleolimnol.*, 50, 57-70, 2013.

769 Korte, M., Donadini, F., Constable, C.G.: Geomagnetic field for 0–3 ka: 2. A new series of  
770 time-varying global models, *Geochemistry Geophysics Geosystems (G3)*, 10, Q06008, doi:  
771 10.1029/2008GC002297, 2009.

772 Lamb, H. H.: The early medieval warm epoch and its sequel, *Palaeogeogr. Palaeoclimatol.*  
773 *Palaeoecol.*, 1, 13–37, 1965.

774 Lambert, J, and Levret-Albaret, A.: Mille ans de séismes en France. Catalogues d'épicentres,  
775 paramètres et references, Ouest-Editions, Presses Académiques, Nantes. 1996.

776 Lapointe, F., Francus, P., Lamoureaux, S.F., Saïd, M. and Cuvén, S.: 1,750 years of large  
777 rainfall events inferred from particle size at East Lake, Cape Bounty, Melville Island, Canada,  
778 *Journal of Paleolimnology*, 48(1), 159–173, 2012.

779 Lionello, P., Abrantes, F., Congedi, L., Dulac, F., Gacic, M., Gomis, D., Goodess, C., Hoff,  
780 H., Kutiel, H., Luterbacher, J., Planton, S., Reale, M., Schröder, K., Struglia, M.V., Toreti, A.,  
781 Tsimplis, M., Ulbrich, U. and Xoplaki, E.: Introduction: Mediterranean Climate: Background  
782 Information in Lionello P. (Ed.) *The Climate of the Mediterranean Region. From the Past to*  
783 *the Future*, Amsterdam: Elsevier (Netherlands), XXXV-XXXX, 2012.

784 Lurcock, P. C. and Wilson, G. S.: PuffinPlot: A versatile, user-friendly program for  
785 paleomagnetic analysis, *Geochemistry, Geophysics, Geosystems*, 13, Q06Z45, 2012.

786 Luterbacher, J., García-Herrera, R., Akcer-On, S., Allan, R., Alvarez-Castro, M. C., Benito,  
787 G., Booth, J., Büntgen, U., Cagatay, N., Colombaroli, D., Davis, B., Esper, J., Felis, T.,  
788 Fleitmann, D., Frank, D., Gallego, D., Garcia-Bustamante, E., Glaser, R., González-Rouco,  
789 J.F., Goosse, H., Kiefer, T., Macklin, M.G., Manning, S., Montagna, P., Newman, L., Power,  
790 M.J., Rath, V., Ribera, P., Riemann, D., Roberts, N., Sicre, M., Silenzi, S., Tinner, W.,  
791 Valero-Garces, B., van der Schrier, G., Tzedakis, C., Vannièrè, B., Vogt, S., Wanner, H.,  
792 Werner, J.P., Willett, G., Williams, M.H., Xoplaki, E., Zerefos, C.S. and Zorita, E.: A review  
793 of 2000 years of paleoclimatic evidence in the Mediterranean, In: Lionello, P. (Ed.), *The*

794 Climate of the Mediterranean region: from the past to the future, Elsevier, Amsterdam, The  
795 Netherlands, 87-185, 2012.

796 Miramont, C., Jorda, M. and Pichard, G.: Évolution historique de la morphogénèse et de la  
797 dynamique fluviale d'une rivière méditerranéenne : l'exemple de la moyenne Durance  
798 (France du sud-est), *Géographie physique et Quaternaire*, 52(3), 381-392, 1998.

799 Moernaut, J., M. De Batist, F. Charlet, K. Heirman, E. Chapron, M. Pino, R. Brümmer and R.  
800 Urrutia, Giant earthquakes in South-Central Chile revealed by Holocene mass-wasting events  
801 in Lake Puyehue, *Sediment. Geol.*, 195, 239–256, 2007.

802 Moernaut, J., Van Daele, M., Heirman, K., Fontijn, K., Strasser, M., Pino, M., Urrutia R., and  
803 De Batist, M.: Lacustrine turbidites as a tool for quantitative earthquake reconstruction: New  
804 evidence for a variable rupture mode in south central Chile, *J. Geophys. Res. Solid Earth*,  
805 119, doi:10.1002/2013JB010738, 2014.

806 Monecke, K., Anselmetti, F.S., Becker, A., Sturm, M. and Giardini, D.: The record of historic  
807 earthquakes in lake sediments of Central Switzerland, *Tectonophysics*, 394, 21–40, 2004.

808 Munich Re Group: Annual Review: Natural Catastrophes 2002, Munich Re Group, Munich,  
809 Germany, 2003.

810 Moreno, A., Valero-Garces, B.L., Gonzalez-Samperiz, P. and Rico, M.: Flood response to  
811 rainfall variability during the last 2000 years inferred from the Taravilla Lake record (Central  
812 Iberian Range, Spain), *J. Palaeolimnol.*, 40, 943–961, 2008.

813 Noren, A.J., Bierman, P.R., Steig, E.J., Lini, A. and Southon, J.: Millennial-scale storminess  
814 variability in the northeastern United States during the Holocene epoch, *Nature*, 419, 821-824,  
815 2002.

816 Osleger, D.A., Heyvaert, A.C., Stoner, J.S. and Verosub, K.L.: Lacustrine turbidites as  
817 indicators of Holocene storminess and climate: Lake Tahoe, California and Nevada, *J*  
818 *Paleolimnol.*, 42:103–122, 2009.

819 Page, M.J., Trustrum, N.A. and DeRose, R.C.: A high resolution record of storm-induced  
820 erosion from lake sediments, New Zealand, *Journal of Paleolimnology*, 11, 333-348, 1994.

821 Parajka, J., Kohnová, S., Bálint, G., Barbuc, M., Borga, M., Claps, P., Cheval, S., Dumitrescu,  
822 A., Gaume, E., Hlavčová, K., Merz, R., Pfaundler, M., Stancalie, G., Szolgay, J., Blöschl, G.:  
823 Seasonal characteristics of flood regimes across the Alpine–Carpathian range, *J. of*  
824 *Hydrology*, 394, 78–89, 2010.

825 Passega, R.: Grain-size representation by CM patterns as a geological tool, *J. of Sedimentary*  
826 *Petrology*, 34(4), 830–847, 1964.

827 Plaut, G., Schuepbach, E. and Doctor, M. Heavy precipitation events over a few Alpine sub-  
828 regions and the links with large-scale circulation, 1971–1995, *Climate Research*, 17, 285–302,  
829 2009.

830 Raible, C.C., Yoshimori, M., Stocker, T.F. and Casty, C.: Extreme midlatitude cyclones and  
831 their implications for precipitation and wind speed extremes in simulations of the Maunder  
832 Minimum versus present day conditions. *Clim. Dyn.* 28, 409–423, 2007.

833 Rajczak, J., Pall, P. and Schär, C.: Projections of extreme precipitation events in regional  
834 climate simulations for Europe and the Alpine Region, *J. Geophys. Res. Atm.*, 118, 1–17,  
835 2013.

836 Reimer, P.J., Bard, E., Bayliss, A., Beck, J.W., Blackwell, P.G., Bronk Ramsey, C., Buck,  
837 C.E., Cheng, H., Edwards, R.L., Friedrich, M., Grootes, P.M., Guilderson, T.P., Haflidason,  
838 H., Hajdas, I., Hatt, C., Heaton, T.J., Hogg, A.G., Hughen, K.A., Kaiser, K.F., Kromer, B.,  
839 Manning, S.W., Niu, M., Reimer, R.W., Richards, D.A., Scott, E.M., Southon, J.R., Turney,  
840 C.S.M. and van der Plicht, J.: IntCal13 and MARINE13 radiocarbon age calibration curves 0-  
841 50000 years calBP, *Radiocarbon*, 55(4), 1869–1887, 2013.

842 Russell, J.M., Vogel, H., Konecky, B.L., Bijaksana, S., Huang, Y., Melles, M., Wattrus, N.,  
843 Costa, K. and King, J.W.: Glacial forcing of central Indonesian hydroclimate since 60,000 y  
844 B.P., *Proc .Nat. Acad. Sci.* 111, 5100-5105, 2014.

845 Sauerbrey, M. A., Juschus, O., Gebhardt, A. C., Wennrich, V., Nowaczyk, N. R. and Melles,  
846 M.: Mass movement deposits in the 3.6Ma sediment record of Lake Elgygytgyn, Far East  
847 Russian Arctic, *Climate of the Past* 9, 1949–1967, 2013.

848 Schiefer, E., Gilbert, R. and Hassan, M.A.: A lake sediment-based proxy of floods in the  
849 Rocky Mountain Front Ranges, Canada, *Journal of Paleolimnology*, 45, 137–149, 2011.

850 Schulte, L., Peña, J.C., Carvalho, F., Schmidt, T., Julià, R., Llorca, J. and Veit, H.: A 2600-  
851 year history of floods in the Bernese Alps, Switzerland: frequencies, mechanisms and climate  
852 forcing, *Hydrol. Earth Syst. Sci.*, 19, 3047–3072, 2015.

853 Schwartz, S., Tricart, P., Lardeaux, J.M., Guillot, S. and Vidal, O.: Late tectonic and  
854 metamorphic evolution of the Piedmont accretionary wedge(Queyras Schistes lustrés, western

855 Alps): Evidences for tilting during Alpine collision, *Geol. Soc. Ame. Bull.*, 121, 502-518,  
856 2009.

857 Scotti, O., Baumont, D., Quenet, G. and Levret, A.: The French macroseismic database  
858 SISFRANCE: objectives, results and perspectives, *Annals of Geophysics*, 47(2), 571-581,  
859 2004.

860 Servonnat, J., Yiou, P., Khodri, M., Swingedouw, D., Denvil, S.: Influence of solar  
861 variability, CO<sub>2</sub> and orbital forcing during the last millennium in the IPSLCM4 model, *Clim.*  
862 *Past*, 6, 445-460, 2010.

863 Simonneau, A., Chapron, E., Vanni re, B., Wirth, S.B., Gilli, A., Giovanni, C. Di.,  
864 Anselmetti, F. S., Desmet, M. and Magny M.: Mass-movement and flood-induced deposits in  
865 Lake Ledro, southern Alps, Italy: implications for Holocene palaeohydrology and natural  
866 hazards, *Clim. Past* 9, 825-840, 2013.

867 Sivan, O., Miramont, C., Pichard, G. and Prosper-Laget, V. : Les conditions climatiques de la  
868 torrentialit  au cours du Petit Age Glaciaire de Provence, *Archeologie du Midi Medieval*, 26,  
869 157–168, 2009.

870 Stockmarr, J.: Tablets with spores used in absolute pollen analysis. *Pollen Spores* 13, 615–  
871 621, 1971.

872 St ren, E.N., Olaf Dahl, S., Nesje, A. and Paasche  .: Identifying the sedimentary imprint of  
873 high-frequency Holocene river floods in lake sediments: development and application of a  
874 new method, *Quat. Sci. Rev.*, 29, 3021-3033, 2010.

875 Strasser, M., Hilbe, M. and Anselmetti, F.S.: Mapping basin-wide subaquatic slope failure  
876 susceptibility as a tool to assess regional seismic and tsunami hazards, *Mar. Geophys. Res.*,  
877 32, 331–347, 2011.

878 Sturm, M. and Matter, A.: Turbidites and varves in Lake Brienz (Switzerland): deposition of  
879 clastic detritus by density currents, *Int. Assoc. Sedimentol. Spec. Publ.*, 2, 147–168, 1978.

880 Swierczynski, T., Lauterbach, S., Dulski, P., Delgado, J., Merz, B. and Brauer, A.: Mid- to  
881 late Holocene flood frequency changes in the northeastern Alps as recorded in varved  
882 sediments of Lake Mondsee (Upper Austria), *Quat. Sci. Rev.*, 80, 78–90, 2013.

883 Thorndycraft, V.R. and Benito, G.: Late Holocene chronology of Spain: the role of climatic  
884 variability and human impact, *Catena*, 66, 34–41, 2006.

885 Torres, N.T., Och, L.M., Hauser, P.C., Furrer, G., Brandl, H., Vologina, E., Sturm, M., and  
886 Bürgmann, H. z Müller, B.: Early diagenetic processes generate iron and manganese oxide  
887 layers in the sediments of Lake Baikal, Siberia, *Env. Sci.: Processes Impacts*, 16, 879–889,  
888 2014.

889 Trigo, I.F. and Davies, T.D.: Decline in Mediterranean rainfall caused by weakening of  
890 Mediterranean cyclones, *Geophysical Research Letters*, 27(18), 2913–2916, 2000.

891 Van Daele, M., Versteeg, W., Pino, M., Urrutia, R. and De Batist, M.: Widespread  
892 deformation of basin-plain sediments in Aysén fjord [Chile] due to impact by earthquake-  
893 triggered, onshore-generated mass movements, *Marine Geol.*, 337, 67–79, 2013.

894 Van Daele, M., Moernaut, J., Doom, L. , Boes, E. , Fontijn, K., Heirman, K. , Vandoorne, W.,  
895 Hebbeln, D., Pino, M., Urrutia, R., Brümmer, R. and De Batist, M.: A comparison of the  
896 sedimentary records of the 1960 and 2010 great Chilean earthquakes in 17 lakes: Implications  
897 for quantitative lacustrine palaeoseismology, *Sedimentology*, 62(5): 1466–1496, 2015.

898 Van Geel, B. and Aptroot, A.: Fossil ascomycetes in Quaternary deposits. *Nova Hedwig* 82,  
899 313–329, 2006.

900 Van Geel, B., Buurman, J., Brinkkemper, O., Schelvis, J., Aptroot, A., van Reenen, G. and  
901 Hakjbilj, T.: Environmental reconstruction of a Roman period settlement site in Uitgeest (The  
902 Netherlands), with special reference to coprophilous fungi. *J. Archaeol. Sci.* 30, 873–883,  
903 2003.

904 Wilhelm, B., Arnaud, F., Sabatier, P., Crouzet, C., Brisset, E., Chaumillon, E., Disnar, J.R.,  
905 Guiter, F., Malet, E., Reyss, J.L., Tachikawa, K., Bard, E. and Delannoy, J.J.: 1400 years of  
906 extreme precipitation patterns over the Mediterranean French Alps and possible forcing  
907 mechanisms, *Quat. Res.*, 78, 1–12, 2012a.

908 Wilhelm, B., Arnaud, F., Enters, D., Allignol, F., Legaz, A., Magand, O., Revillon, S.,  
909 Giguet-Covex, C. and Malet, E.: Does global warming favour the occurrence of extreme  
910 floods in European Alps? First evidences from a NW Alps proglacial lake sediment record,  
911 *Clim. Change.*, 113, 563–581, 2012b.

912 Wilhelm, B., Arnaud, F., Sabatier, P., Magand, O., Chapron, E., Courp, T., Tachikawa, K.,  
913 Fanget, B., Malet, E., Pignol, C., Bard, E. and Delannoy, J.J.: Palaeoflood activity and climate  
914 change over the last 1400 years recorded by lake sediments in the NW European Alps, *J.*  
915 *Quat. Sci.*, 28, 189–199, 2013.

916 Wilhelm, B., Sabatier, P. and Arnaud, F.: Is a regional flood signal reproducible from lake  
917 sediments? *Sedimentology*, 62(4), 1103–1117. 2015.

918 Wirth S.B., Glur, L., Gilli, A. and Anselmetti, F.S.: Holocene flood frequency across the  
919 Central Alps – solar forcing and evidence for variations in North Atlantic atmospheric  
920 circulation, *Quatern. Sci. Rev.*, 80, 112–128, 2013a.

921 Wirth, S.B., Gilli, A., Simonneau, A., Ariztegui, D., Vannière, B., Glur, L., Chapron, E.,  
922 Magny, M. and Anselmetti, F.S.: A 2000-year long seasonal record of floods in the southern  
923 European Alps. *Geophys. Res. Let.*, 40(15), 4025-4029, 2013b.

924

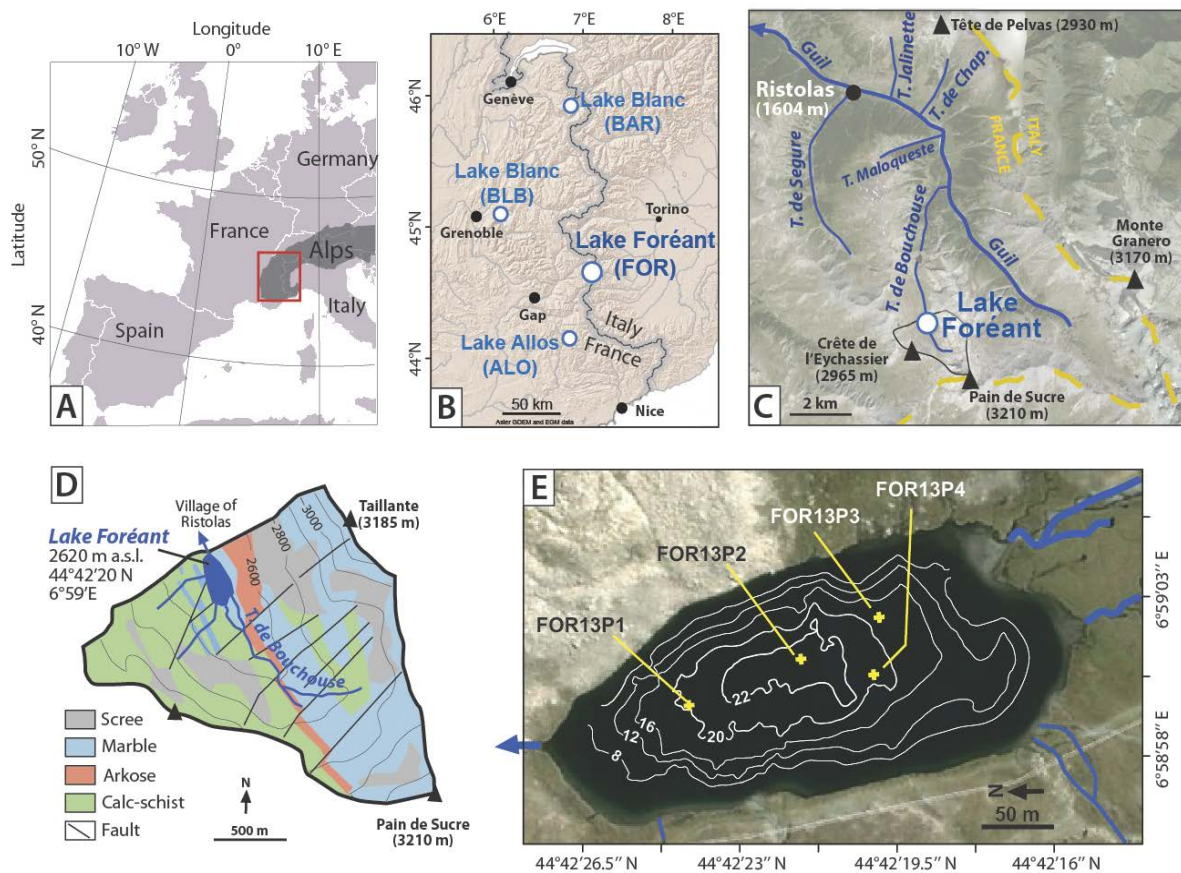
925

BE nr.	Core	Core depth (cm)	Core depth in core FOR13P2 (cm)	Event-free depth in core FOR13P2 (cm)	Material	<sup>14</sup> C yrs. BP	Cal yrs. BP (±2σ)	Cal yrs. AD (±2σ)
2094.1.1	FOR13P4	84-85	82-83	33	Terrestrial plant remains	650 ± 18	561-665	1285-1389
2095.1.1	FOR13P4	109-111	106-108	46 ± 0.5		1052 ± 33	923-1052	898-1027
2096.1.1	FOR13P4	113-115	110-112	47 ± 0.5		1242 ± 66	1004-1292	658-946

926

927 Table 1. Radiocarbon dates of core FOR13P4. We calculated the event-free sedimentary  
 928 depth by removing the graded beds, which were considered to be instantaneous deposits. See  
 929 text for explanation, nature of samples and calibration procedures.

930

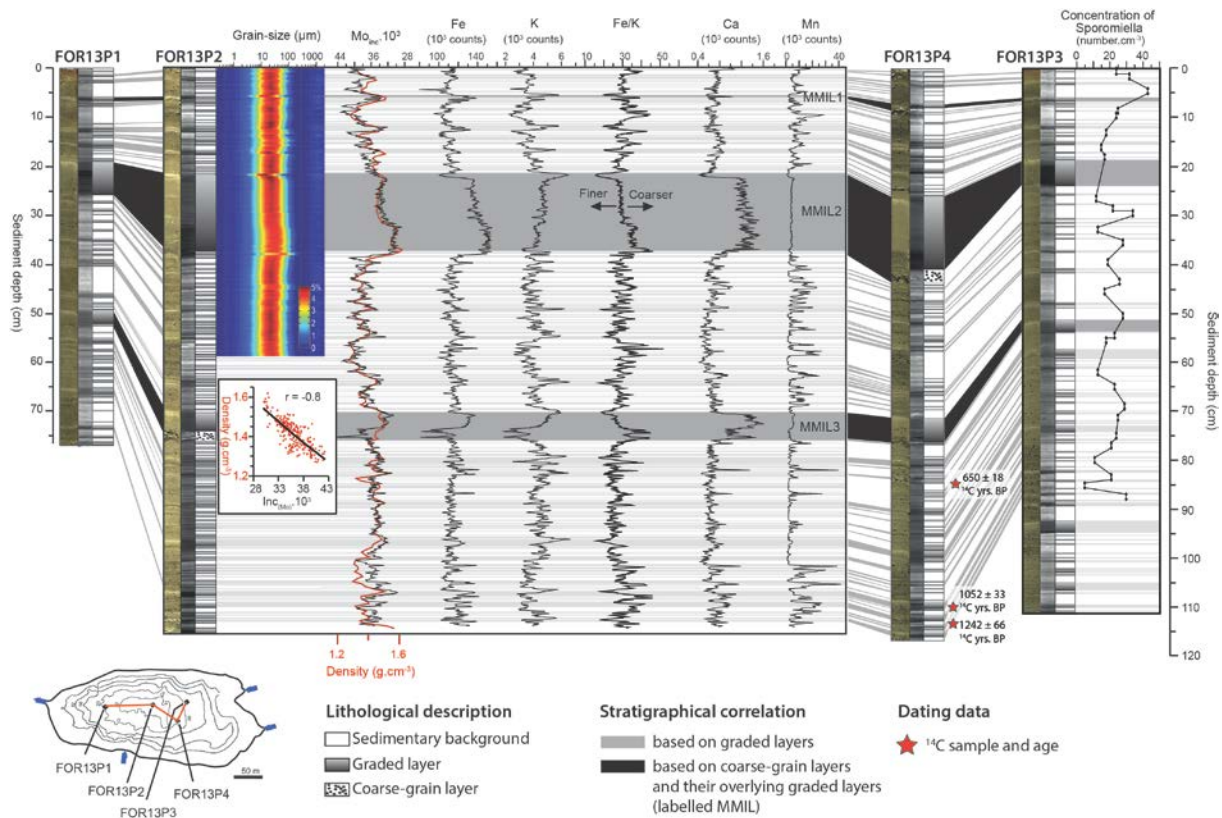


931

932 Figure 1. (A) Location of Lake Foréant in the Western Alps, (B) compared to the locations of  
 933 the previously studied Lakes Blanc (BLB, Wilhelm et al., 2012b; BAR, Wilhelm et al., 2013)  
 934 and Lake Allos (ALO, Wilhelm et al., 2012a). (C) Location of the Foréant catchment area in  
 935 the hydrological network flowing to the village of Ristolas. (D) Geological and  
 936 geomorphological characteristics of the Foréant catchment area. (E) Bathymetric map of Lake  
 937 Foréant and coring sites.

938

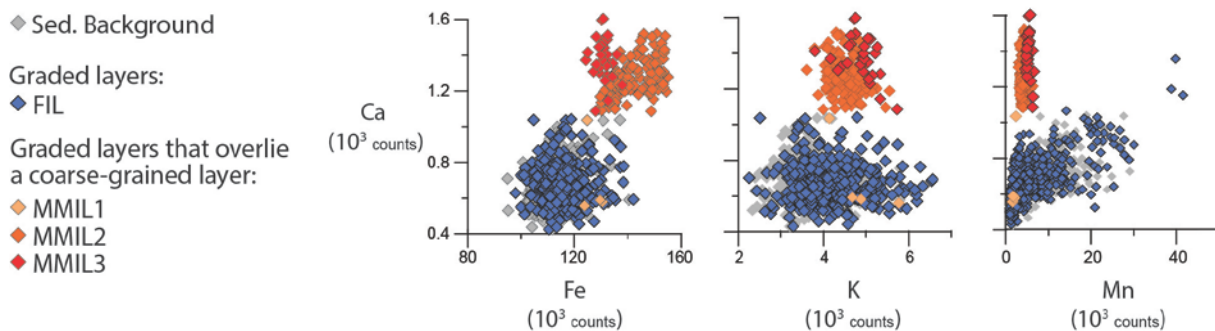




939

940 Figure 2. Lithological descriptions of cores and stratigraphic correlations based on  
 941 sedimentary facies. For each core, a photography (left), a X-ray image (center) and a  
 942 stratigraphic log is shown (right). <sup>14</sup>C samples are indicated by red stars. Variability in grain-  
 943 size distribution and geochemical elements (Fe, K, Ca and Mn) is shown for the core  
 944 FOR13P2.  $\text{Mo}_{\text{inc}}$  used as a high-resolution proxy of density is shown close to the density  
 945 measurements performed by gamma-ray attenuation. Variability in Sporormiella concentration  
 946 is shown for core FOR13P3.

947

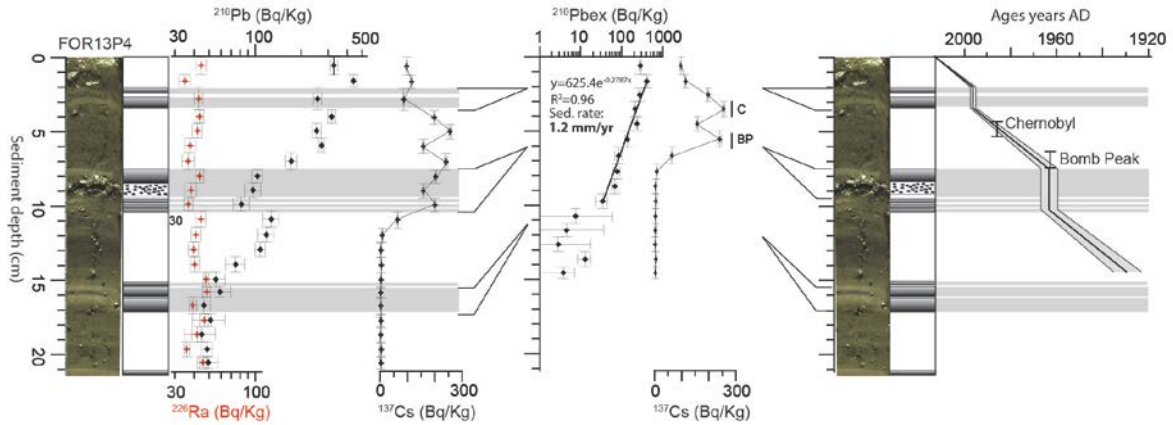


948

949 Figure 3. To illustrate the different geochemical characteristics of the sedimentary  
 950 background and the graded layers, their Ca intensities were plotted against their Fe, K and Mn

951 intensities. FIL refers to flood- and MMIL to mass-movement-induced layers. The different  
952 MMILs are labelled according to figure 2.

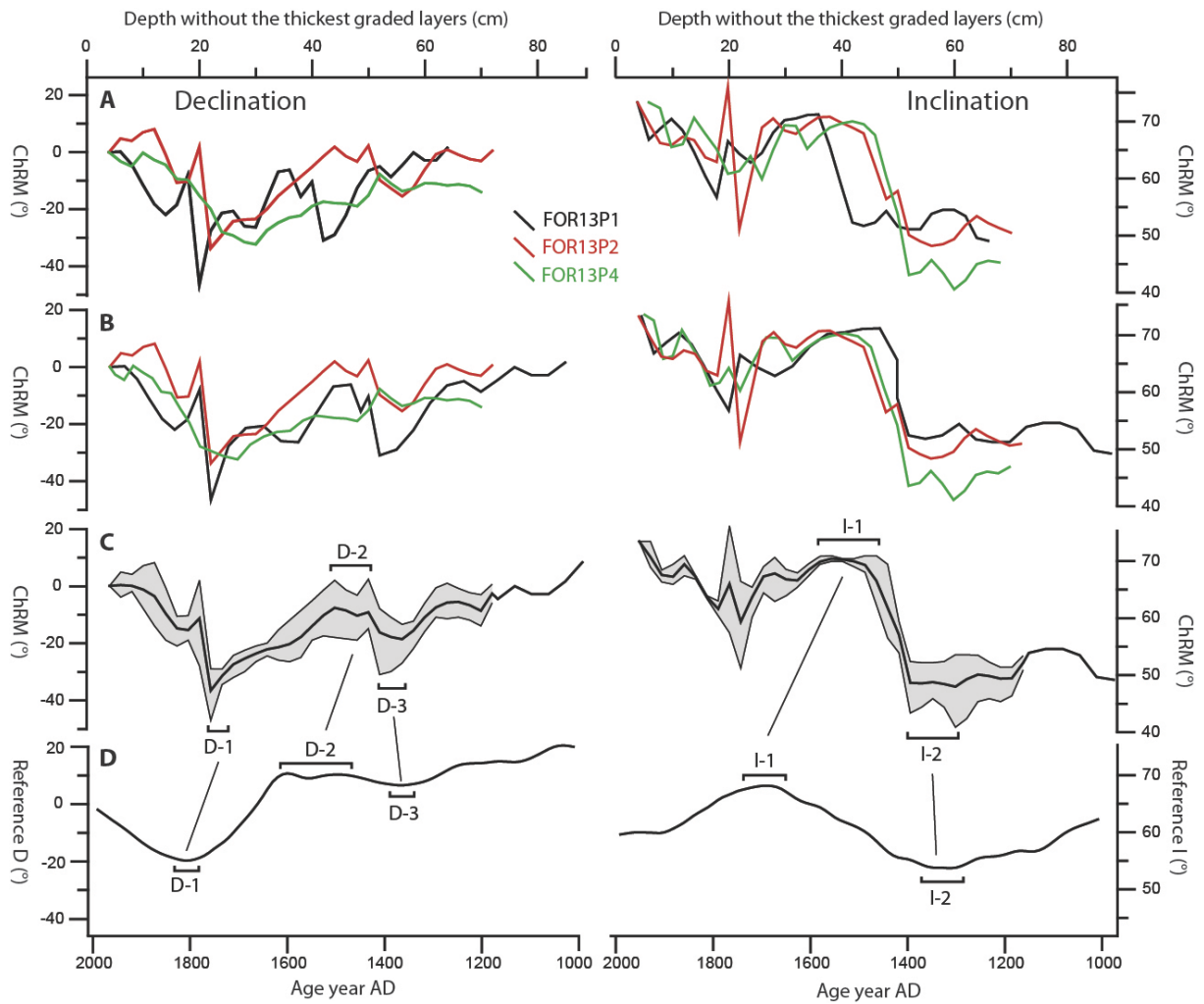
953



954

955 Figure 4. (A)  $^{226}\text{Ra}$ ,  $^{210}\text{Pb}$  and  $^{137}\text{Cs}$  profiles for core ALO09P12. (B) Application of a CFCS  
956 model to the event-free sedimentary profile of  $^{210}\text{Pb}$  in excess (without the thick graded beds  
957 considered as instantaneous deposits). (C) Resulting age–depth relationship with  $1\sigma$   
958 uncertainties and locations of the historic  $^{137}\text{Cs}$  peaks supporting the  $^{210}\text{Pb}$ -based ages. C  
959 corresponds to the historic  $^{137}\text{Cs}$  peak of Chernobyl (AD 1986) and MP to the maximum  $^{137}\text{Cs}$   
960 peak of the nuclear fallout (AD 1963).

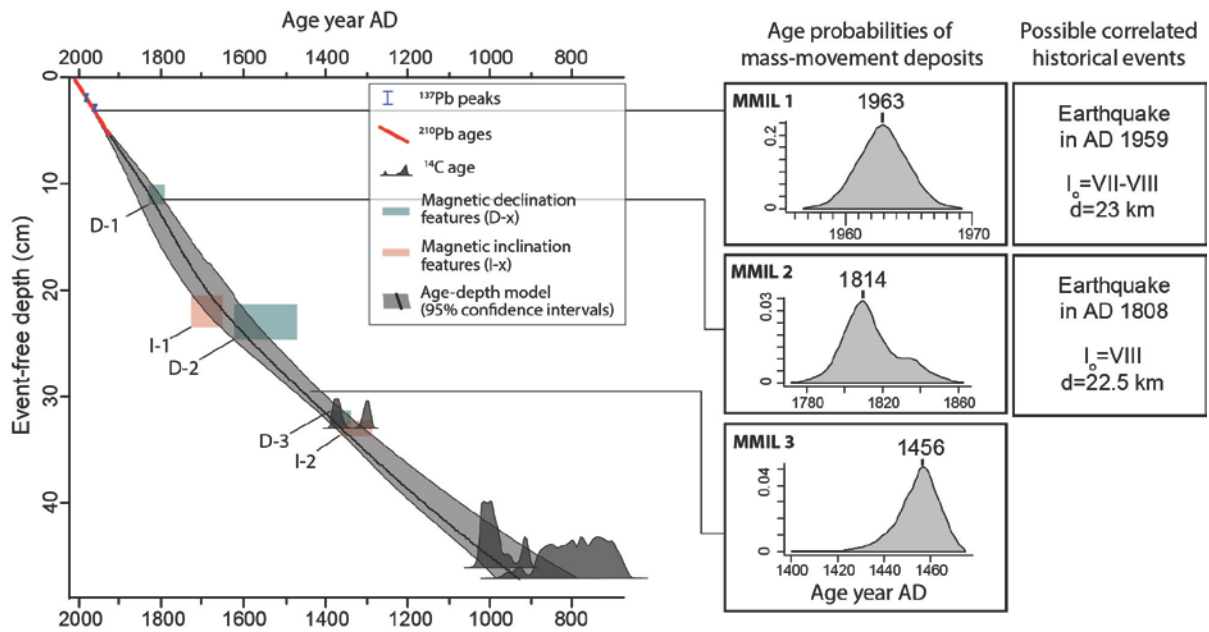
961



962

963 Figure 5. (A) Raw declination and inclination profiles of cores FOR13P1, FOR13P2 and  
 964 FOR13P4. (B) The same profiles after removal of the thickest graded beds (interpreted as  
 965 event layers) and adjustment of the different specific-core depths to a common reference  
 966 depth. (C) Average of profiles shown in (B). (D) Correlation to the ARCH3.4k model  
 967 reference curve of declination and inclination (Donadini et al., 2009; Korte et al., 2009).  
 968 ChRM means characteristic remanent magnetization. The well-correlated declination and  
 969 inclination features are labelled D-x and I-x, respectively.

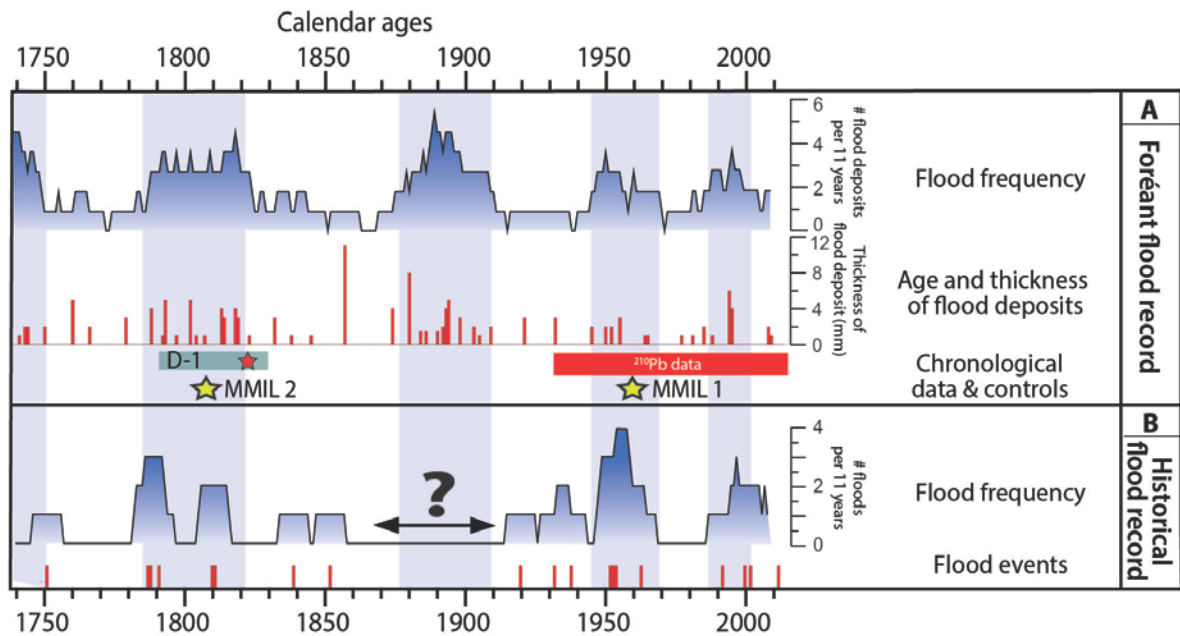
970



971

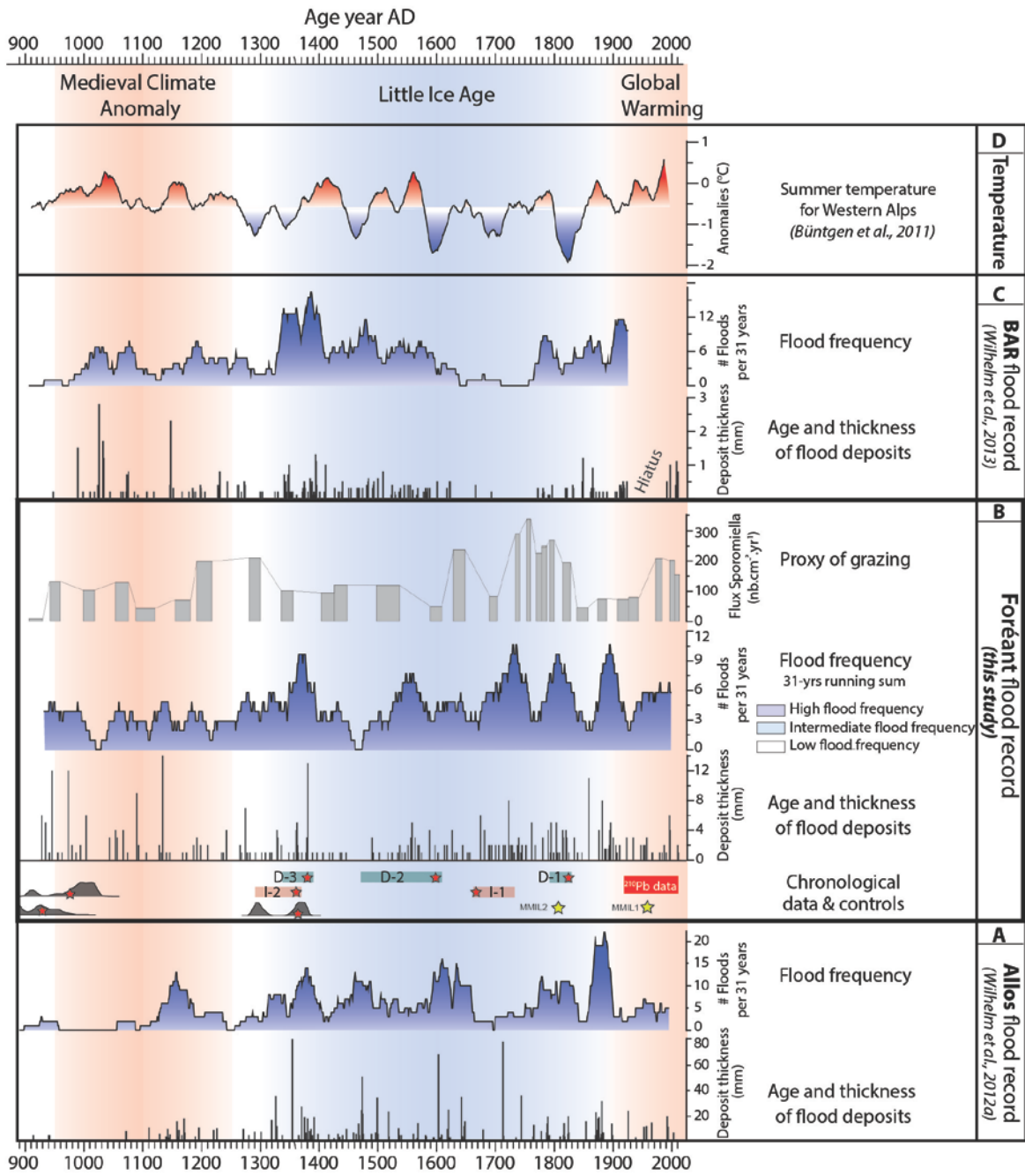
972 Figure 6. Age–depth model for core FOR13P2 calculated using the “clam” R-code package,  
 973 combining historic  $^{137}\text{Cs}$  peaks,  $^{210}\text{Pb}$  ages, calibrated  $^{14}\text{C}$  ages and magnetic features on the  
 974 left side. Probability distribution frequencies of mass-movement ages and possible  
 975 correlations to historical earthquakes on the right side.

976



977

978 Figure 7. Comparison over the last 250 years of the reconstructed Foréant flood frequency  
 979 (11-yr running sum) and intensity (thickness of flood deposits) with the frequency (11-yr  
 980 running sum) of historical floods at Ristolas. The question mark refers to a possible gap in the  
 981 historical data.



982

983 Figure 8. Comparison over the last millennium of (B) the reconstructed Foréant flood  
 984 frequency (31-yr running average) and intensity (thickness of flood deposits) with (A) the  
 985 Allos flood record from the southern French Alps (Wilhelm et al., 2012a), (C) the BAR flood  
 986 record from the northern French Alps (Wilhelm et al., 2013) and (D) the tree-ring-based  
 987 summer temperature for the European Alps (Büntgen et al., 2011). The reconstructed  
 988 *Sporomiella*-type flux is also shown next to the Foréant flood record to highlight potential  
 989 human impacts (i.e. grazing) on the erosion processes that might bias the flood record. The  
 990 red stars below the Foréant record show the chronological markers with their 2-sigma  
 991 uncertainty ranges.

## Supplementary Material

### **A millennium of flood activity at the climatic boundary between Atlantic and Mediterranean influences**

B. Wilhelm<sup>1,2</sup>, H. Vogel<sup>2</sup>, C. Crouzet<sup>3</sup>, D. Etienne<sup>4,5</sup>, F. Anselmetti<sup>2</sup>

<sup>1</sup>Univ. Grenoble Alpes, LTHE, F-38000 Grenoble, France

<sup>2</sup>Institute of Geological Sciences and Oeschger Centre for Climate Change Research, Univ. of Bern, CH-3012 Bern, Switzerland

<sup>3</sup>Univ. Savoie Mont Blanc, CNRS, ISTERre, F-73376 Le Bourget-du-Lac, France

<sup>4</sup>UMR INRA 42 CARTELE, Univ. Savoie Mont Blanc, F-73376 Le Bourget du Lac, France

<sup>5</sup>INRA, CARTELE, F-74200 Thonon-les-Bains, France

#### **Chronology: detailed methods for palaeomagnetic investigations**

Palaeomagnetic investigations were performed at the CEREGE laboratory (Aix-Marseille University) on cores FOR13P1, FOR13P2 and FOR13P4 using u-channels sub-samples. The natural remanent magnetization (NRM) was progressively demagnetized using alternating fields with 10, 20, 30, 40, 60, 80 and 100 mT steps. In order to distinguish different mineralogical and grain-size fractions within the magnetic components, two types of laboratory remanent magnetizations were conducted: Isothermal Remanent Magnetization (IRM) and Anhyseretic Remanent Magnetization (ARM). ARM was produced in-line along the u-channel axis, using a 100 mT alternating field with a superimposed 0.05 mT steady field. IRM was obtained by passing the u-channels through two different Halbach cylinders that develop fields of 1 and 0.3 T, respectively (Rochette et al., 2001). For ARM and IRM1T, demagnetization was done following steps of 10, 20, 30, 40, 60, 80 and 100 mT. The magnetizations have been measured before alternating-field treatment and after each step using the 3-axis 2-G enterprise cryogenic magnetometer located in a shielded room. Additionally, anisotropy of magnetic susceptibility has been measured using AGICO MFK1-FA Kappabridge (spinning specimen method) to control the preservation of the sedimentary

fabric. The susceptibility ellipsoid is defined by three eigenvectors ( $K_{max}$ ,  $K_{int}$  and  $K_{min}$ ). The magnetic fabric is usually comparable to the sediment fabric with inclination of the  $K_{min}$  close to the vertical (Borradaile, 1988; Rochette et al., 1992; Tarling and Hrouda, 1993).

<b>Flood date</b>	<b>Affected rivers</b>	<b>Spatial extent of the flood</b>	<b>Victim</b>	<b>Damage</b>	<b>Disruptions</b>	<b>Details on the hydro-meteorological causes</b>
> 3 September 2012	Guil	Ristolas and villages downstream	N	Y	Y	Easterlies winds with heavy rainfalls in the upper part of catchment
28 May 2008	Guil	Ristolas and villages downstream	Y	Y	Y	Heavy rainfall event
13 June 2002	Torrents of Segure and other	Ristolas	N	N	N	Heavy rainfalls mainly in the upper part of the catchment
> 15 July 2002	Guil	Ristolas and villages downstream	N	Y	Y	Easterlies winds with heavy rainfalls in the upper part of the catchment
> 15 October 2000	Guil and other	Ristolas and villages downstream	N	Y	N	5 days of heavy rainfalls with increased rainfall depths the last 2 days
13 June 2000	Guil and Torrent of Segure	Ristolas and villages downstream	N	Y	Y	Heavy rainfalls mainly in the upper part of the catchment
> July 1992	Torrent of Bouchouse	Ristolas	N	Y	Y	Violent thunderstorms
11 June 1978	Guil	Ristolas and villages downstream	N	Y	U	
5 May 1973	Guil	Ristolas and villages downstream	N	Y	U	
> 1 November 1963	Undefined	Ristolas	N	Y	U	
21 May 1959	Guil	Ristolas and villages downstream	N	Y	Y	
> Summer 1959	Guil	Ristolas and villages downstream	N	U	Y	
13 June 1957	Guil and Torrent of Segure	Ristolas and villages downstream	N	Y	Y	Heavy rainfalls, thunderstorm, snowmelt
> October 1953	Torrent of Jalinette	Ristolas	N	Y	Y	Heavy rainfall event
> 29 Sept. 1953	Guil	Ristolas and villages downstream	N	Y	Y	Heavy rainfall event during 3 days
> 1 July 1953	Torrent of Jalinette	Ristolas	N	Y	Y	
8 June 1953	Guil	Ristolas and villages downstream	N	Y	Y	Violent thunderstorms and snowmelt
14 May 1948	Guil	Ristolas and villages downstream	Y	Y	Y	Rainfall depth of 244 mm in 3 days, with snowmelt
> 4 August 1938	Torrent of Segure	Ristolas	N	Y	Y	Violent thunderstorms
1932	Torrent of Maloqueste	Ristolas	N	Y	U	
> 9 July 1932	Guil	Ristolas and villages downstream	N	Y	Y	
> 1 September 1920	Guil	Ristolas and villages downstream	N	Y	Y	
29 May 1856	Guil	Ristolas and villages downstream	N	U	U	Heavy rainfalls over a long period before the flood event
> 6 August 1852	Guil	Ristolas and villages downstream	N	Y	Y	Heavy rainfall events
> 15 October 1839	Guil	Ristolas and villages downstream	N	Y	U	Heavy rainfall events
> 13 Sept. 1810	Guil and Torrent of Segure	Ristolas and villages downstream	N	Y	Y	Heavy rainfall events during 8 days
> 13 October 1810	Guil	Ristolas and villages downstream	N	Y	Y	
> 10 October 1791	Guil and Torrent of Chapelle	Ristolas and villages downstream	N	Y	Y	
> 9 October 1790	Guil	Ristolas and villages downstream	N	Y	Y	
1789	Guil	Ristolas and villages downstream	N	Y	Y	
> 07 Sept. 1788	Guil	Ristolas and villages downstream	N	Y	Y	
> 7 September 1787	Guil	Ristolas and villages downstream	N	Y	U	
> 4 October 1751	Guil	Ristolas and villages downstream	N	U	U	Heavy rainfall events



**Table S1.** List of historical flood events which runs through the village of Ristolas, located 8 km downstream from Lake Foréant (from the free-access database of the ONF-RTM, <http://rtm-onf.ifn.fr/>). The arrows in the first row highlight the floods that occurred in summer and fall, i.e. that may be recorded in the lake sediments because this period corresponds to the ice-free season of Lake Foréant. N means No, Y means Yes and U, Uncertain.

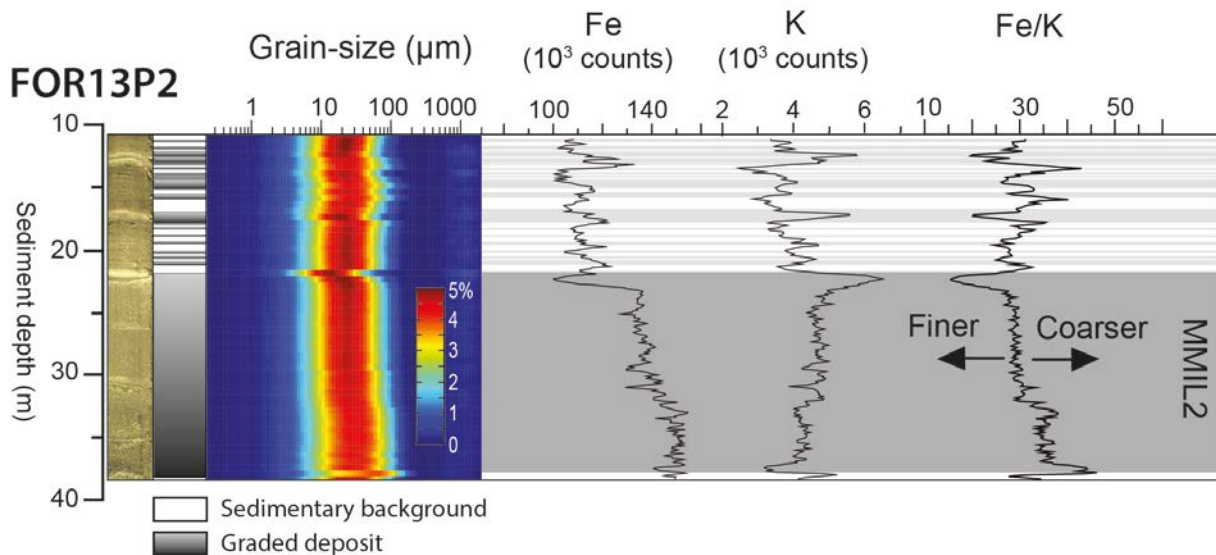


**Fig. S1.** Zoom of the grain-size variability and associated geochemical proxy for core FOR13P2. Refer to Figure 2 and to the main text for details.

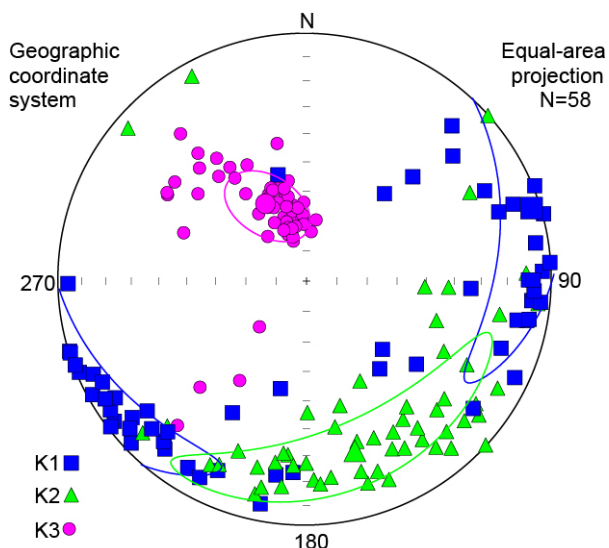


**Fig. S2.** Results of Anisotropy of Magnetic Susceptibility for core FOR13P4: stereo plot of the main axes direction. Notice that the K3 is well grouped and close to the vertical except some points associated with MMITs.

FOR13 P3 88 cm  
MAD = 2,17  
Units:  $2 \cdot 10^{-4}$  A/m

FOR13 P1 10 cm  
MAD=1,67  
Unit:  $10^{-4}$  A/m

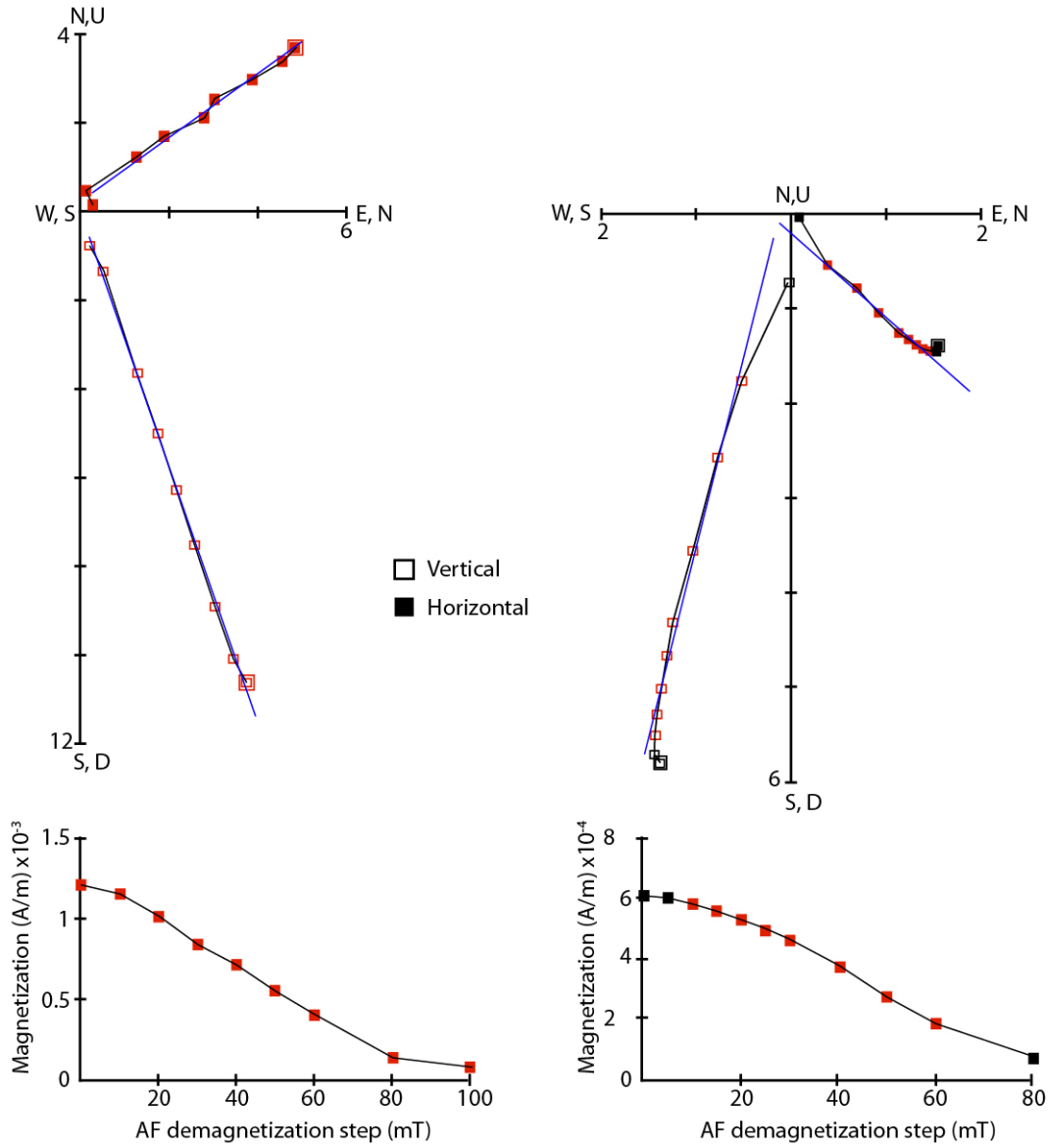


**Fig. S3.** Example of stepwise alternating field demagnetization of NRM (orthogonal vector projections and intensity curves) for representative samples. Solid (open) symbols are horizontal (vertical) plane projections.

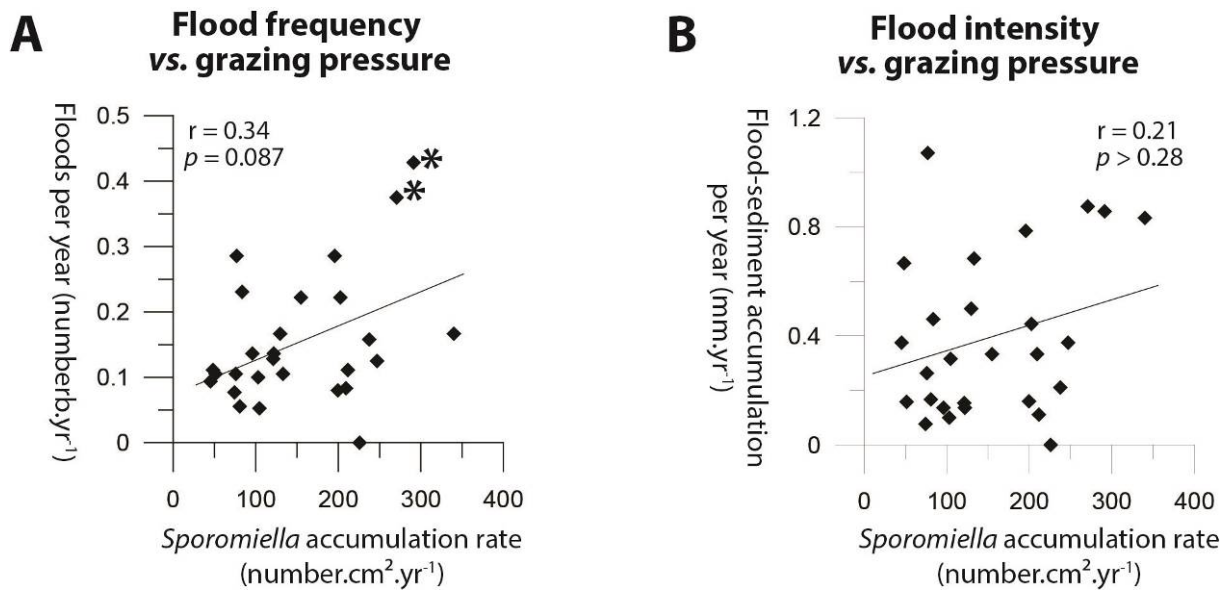


**Fig. S4.** Representation and correlation coefficients ( $r$ ) of relations between (A) *Sporormiella* accumulation rates (number.cm<sup>2</sup>.yr<sup>-1</sup>) and floods frequency (nb.yr<sup>-1</sup>), and between (B) *Sporormiella* accumulation rates (number. cm<sup>2</sup> yr<sup>-1</sup>) and flood-sediment accumulation (mm.years<sup>-1</sup>). The stars identified two samples, dated from 1734 to 1760 AD, with both high grazing pressure and high flood frequency. Levels of significance ( $p$  values) were determined using a Spearman-test.

#### References

- Rochette, P., Jackson, M., Aubourg, C.: Rock magnetism and the interpretation of anisotropy of magnetic susceptibility, *Reviews of Geophysics* 30 (3), 209–226, 1992.
- Rochette, P., Vadeboin, F., Clochard, L.: Rock magnetic applications of Halbach cylinders, *Physics of the Earth and Planetary Interiors* 126, 109–117, 2001.
- Borradaile, G.: Magnetic susceptibility, petrofabrics and strain, *Tectonophysics*, 156, 1–20, 1988.
- Tarling, D.H., Hrouda, F.: *The Magnetic Anisotropy of Rocks*, Chapman & Hall, London (218 pp.), 1993.